Title: Transcriptional signatures of participant-derived neural progenitor cells and neurons implicate altered Wnt signaling in Phelan McDermid syndrome and autism

Authors: Michael S. Breen[1, 2, 3, 5, 8*]; Andrew Browne[1, 2*]; Gabriel E. Hoffman[3, 5, 8]; Sofia Stathopoulos[1, 2]; Kristen Brennand[2, 3, 4, 7,8]; Joseph D. Buxbaum[1, 2, 3, 4, 6, 7†‡]; Elodie Drapeau[1, 2†]

Affiliations: Seaver Autism Center for Research and Treatment[1], Department of Psychiatry[2], Department of Genetics and Genomic Sciences[3], Nash Family Department of Neuroscience[4]; Icahn Institute for Data Science and Genomic Technology[5], Friedman Brain Institute[6], Mindich Child Health and Development Institute[7], Pamela Sklar Division of Psychiatric Genomics[8], Icahn School of Medicine at Mount Sinai, New York, NY, 10029 USA.

Keywords: neural progenitor cells, neurons, stem cells, RNA-sequencing, autism spectrum disorder

*Both first authors contributed equally to this manuscript.

†Both last authors contributed equally to this manuscript.

‡ Corresponding author.

Main Tables: 2

Main Figures: 4

Supplemental Tables: 4

Supplemental Figures: 11

ABSTRACT

Background: Phelan-McDermid syndrome (PMS) is a rare genetic disorder with high risk of autism spectrum disorder (ASD), intellectual disability and language delay, and is caused by 22q13.3 deletions or mutations in the *SHANK3* gene. To date, the molecular and pathway changes resulting from *SHANK3* haploinsufficiency in PMS remain poorly understood. Uncovering these mechanisms is critical for understanding pathobiology of PMS and, ultimately, for the development of new therapeutic interventions.

Methods: We developed human induced pluripotent stem cell (hiPSC)-based models of PMS by reprogramming peripheral blood samples from individuals with PMS (n=7) and their unaffected siblings (n=6). For each participant, up to three hiPSC clones were generated and differentiated into induced neural progenitor cells (iNPCs; n=32) and induced forebrain neurons (iNeurons; n=42). Genome-wide RNA-sequencing was applied to explore transcriptional differences between PMS probands and unaffected siblings.

Results: Transcriptome analyses identified 391 differentially expressed genes (DEGs) in iNPCs and 82 DEGs in iNeurons, when comparing cells from PMS probands and unaffected siblings (FDR <5%). Genes under-expressed in PMS were implicated in Wnt signaling, embryonic development and protein translation, while over-expressed genes were enriched for pre- and post-synaptic density genes, regulation of synaptic plasticity, and G-protein-gated potassium channel activity. Gene co-expression network analysis identified two modules in iNeurons that were over-expressed in PMS, implicating postsynaptic signaling and GDP binding, and both modules harbored a significant enrichment of genetic risk loci for developmental delay and intellectual

disability. Finally, PMS-associated genes were integrated with other ASD iPSC transcriptome findings and several points of convergence were identified, indicating altered Wnt signaling, extracellular matrix and glutamatergic synapses.

Limitations: Given the rarity of the condition, we could not carry out experimental validation in independent biological samples. In addition, functional and morphological phenotypes caused by loss of *SHANK3* were not characterized here.

Conclusions: This is the largest human neural sample analyzed in PMS. Genome-wide RNA-sequencing in hiPSC-derived neural cells from individuals with PMS revealed both shared and distinct transcriptional signatures across iNPCs and iNeurons, including many genes implicated in risk for ASD, as well as specific neurobiological pathways, including the Wnt pathway.

INTRODUCTION

Phelan-McDermid syndrome (PMS) is one of the most penetrant and more common single-locus causes of ASD, accounting for ca. 1% of ASD diagnoses [1-3]. PMS is caused by heterozygous 22q13.3 deletions or mutations leading to haploinsufficiency of the *SHANK3* gene [2, 4-6]. Clinical manifestations of PMS include ASD, global developmental delay, severe to profound intellectual disability (ID), motor abnormalities, delayed or absent speech, and epilepsy [2, 6, 7]. *SHANK3* is a scaffolding protein of the post-synaptic density of excitatory synapses and plays a critical role in synaptic function, being a key component in the integration of glutamatergic synaptic signaling [8-14]. A fundamental knowledge gap separates the well-defined clinical impact of *SHANK3* mutations on neurodevelopmental phenotypes and the molecular and cellular mechanisms leading to these phenotypes. Uncovering these mechanisms is critical for identifying drug targets and developing novel intervention strategies for PMS and for subsets of ASD that share related pathobiological mechanisms.

Several studies have utilized murine models to explore the molecular consequences of *SHANK3*-deficiency. We and others have shown that mice with a disruption in *Shank3* have altered glutamatergic signaling and synaptic dysfunction, as well as altered motor, social and repetitive behaviors [11, 15-26]. Studies on a genetically modified Shank3 rat model showed deficits in attention and in long-term social memory, which were attributable to reduced synaptic plasticity in the hippocampal-medial prefrontal cortex pathway [27, 28]. Many of the features of these rodent models reflect deficits similar to those observed in PMS. However, although animals and humans share homologous genes, pathways, and networks, rodents may have limits as models of human

87 neurodevelopment. Specifically, the biological context and integration of molecular pathways
88 differ across species, which can pose an obstacle for drug development and discovery.
89
90 The generation of neuronal cultures from human induced pluripotent stem cells (hiPSCs) has the
91 potential to create translatable and experimentally tractable human neuronal models [29, 30].
92 hiPSCs can be derived directly from participant cells and reprogrammed to differentiate into target
93 cell types of interest, recapitulating the early stages of neurodevelopment *in vitro*, all while
94 retaining the genetics of the original donor. In several studies, hiPSC-derived neurons have been
95 examined from individuals with PMS and show a reduction in the number of synapses in *SHANK3*-
96 deficient neurons, together with impaired dendritic arborization and major deficits in excitatory,
97 but not inhibitory, synaptic activity [31-36]. Isogenic comparisons of CRISPR-engineered
98 heterozygous and homozygous *SHANK3* mutations demonstrated that *SHANK3*-deficiency causes
99 functionally impaired hyperpolarization-activated cation currents, likely through its ability to
100 interact with and organize the hyperpolarization-activated cyclic nucleotide-gated channels that
101 mediate I_h currents [37]. Some studies indicate that excitatory synaptic transmission in PMS
102 neurons can be corrected by restoring *SHANK3* expression, by treating neurons with IGF-1, or by
103 pharmacologically and genetically activating Akt or inhibiting the Cdc2-like kinase 2 activity [31,
104 34, 35]. Amelioration of deficits associated with *SHANK3* haploinsufficiency have also been
105 demonstrated by treating iPSCs with lithium or valproic acid [34].
106
107 Overall, the rodent and hiPSC-based studies consistently confirm that, at the neurophysiological
108 level, PMS leads to a disruption in glutamatergic signaling. A next step would be to identify
109 consistent molecular changes in PMS, specifically, the repertoire of genes and molecular pathways

that are altered in expression as a consequence of *SHANK3*-deficiency. A better understanding of these molecular mechanisms may inform the search for approaches to ameliorate neurobiological and neurophysiological deficits in vitro, with the ultimate goal of advancing treatments for PMS.

The overarching objective of the current study was to identify the transcriptional signatures of *SHANK3*-deficiency in iNPCs and iNeurons by comparing genome-wide RNA-seq gene expression between PMS probands (n=7) and unaffected siblings (n=6). A multi-step analytic approach was applied to: (1) confirm the developmental specificity of our hiPSC neuronal cells; (2) quantify the variance in iNPC and iNeuron transcriptome data that is explained by differences in neural cell types, individual donors and other relevant factors; and (3) identify and characterize candidate genes, molecular pathways and co-regulatory networks associated with PMS in iNPCs and iNeurons. We identify important molecular pathways that both inform pathobiological mechanisms in PMS and suggest approaches for interventions.

MATERIALS AND METHODS

Participants. The study includes 13 participants (**Table 1**, 7 probands and 6 unaffected siblings) enrolled at the Seaver Autism Center for Research and Treatment at the Icahn School of Medicine at Mount Sinai. Individuals were referred through the Phelan-McDermid Syndrome Foundation, ongoing research studies, and communication between families. The study was approved by the Program for the Protection of Human Subjects at the Icahn School of Medicine at Mount Sinai. Parents or legal guardians provided informed consent for participation and publication.

Genetic findings. The mutation in patient 1 was identified through clinical WES by the Medical Genetics Laboratory at the Baylor College of Medicine. Deletions in patients 2-7 were identified as follows: Patient 2, FISH and chromosome microarray (CMA) by Signature Genomics; patient 3, CMA by the Genetics Laboratory at the University of Oklahoma Health Sciences Center; patient 4, FISH by Quest Diagnostic and CMA by the Shaare Zedek Medical Center, Jerusalem; patient 5, CMA at the UCSF Benioff Children's Hospital Oakland; patient 6, CMA by the Mount Sinai Genetic Testing Laboratory; and, patient 7, karyotyping and custom OGT 22q array by cytogenic laboratory of the Greenwood Genetic Center.

Variants were annotated according to the Human Genome Variation Society guidelines. As reported previously, the human genome reference assembly (GRCh37/hg19 and GRCh38/hg38) is missing the beginning of exon 11 (NM_033517.1:c.1305_1346, 5′-cccgagcgggcccggcggccccggccccgcgcccggccccgg-3′, coding for 436-PSGPGGPGPAPGPG-449). We numbered nucleotide and amino acid positions according to the *SHANK3* RefSeq mRNA (NM_033517.1) and protein (NP_277052.1) sequence, in which this mistake has been corrected.

Variants were interpreted according to the American College of Medical Genetics and Genomics (ACMG) guidelines.

iPSC generation. Blood samples were collected from all participants and used for both DNA isolation (DNeasy Blood and Tissue Kit, Qiagen) and peripheral blood mononuclear cells (PBMCs) extraction (BD Vacutainer CPT Mononuclear Cell Preparation Tubes with Sodium Heparin, BD Biosciences) according to manufacturer's instructions. PBMCs were cultured for 9 to 12 days in an erythroblast enrichment medium [38] to expand the erythroblast population and 2.5×10^5 cells were transduced using recombinant Sendai viral vectors (Cytotune-iPSC 2.0^{TM}, Thermofisher scientific), expressing the four reprogramming factors Oct4, Sox2, Kfl4 and c-Myc, according to manufacturer's instructions. After three days, transduced cells were plated on irradiated mouse embryonic fibroblast (MEFs) and grown for two to three weeks in hiPSC medium until the emergence of individual colonies. Live hiPSCs were labeled by Tra-1-60 immunostaining (R&D systems) and positive clones were manually picked and grown on MEFs using iPSC medium. After reaching passage 10, hiPSC colonies were transitioned to feeder-free conditions using Matrigel-coated plates (Corning) and mTeSR1 medium (Stem Cell Technology) and up to three clones per individual were validated, expanded and cryopreserved.

iPSC validation. All hiPSC lines were assessed for chromosomal abnormalities by performing karyotyping (WiCell). Their identity was confirmed using short-tandem repeat (STR) analysis (WiCell) and comparison with the donor's blood DNA. The potential for self-renewal and pluripotency of the hiPSC lines was assessed by utilizing hiPSC RNA with the Taqman hPSC Scorecard Assay (Thermo Fisher, A15870). For pluripotency, RNA was isolated after random differentiation of iPSCs into embryoid bodies [39] to generate the three primary germ layers. Full elimination of the Sendai virus vectors was confirmed by immunostaining and with the Taqman

hPSC Scorecard Assay. The e-Myco Mycoplasma PCR Detection Kit (Bulldog Bio, 25233) and the MycoAlert Mycoplasma Detection Kit (Lonza, LT07-118) were used to ensure that all the cells used in this study were mycoplasma-free.

Generation of neuronal progenitor cells (iNPCs). iNPCs were induced from passage 16 to P18 hiPSCs using the PSC Neural Induction Medium (Invitrogen) according to the manufacturer's protocol. They were maintained in PSC Neural Expansion Medium up to passage 4 and then transferred to NPC medium (DMEM/F12, N2, B27 without retinoic acid, 1µg/mL natural mouse laminin, 20ng/mL FGF2). At passage 5, NPCs were labelled with Sox2 (Santa Cruz SC-17320, 1:100) and Nestin (ThermoFisher MA1-110, 1:200) antibodies to confirm their cellular identity and validated NPCs were cryopreserved. For RNA isolation, NPCs at passage 6 were seeded into 12-well plates at a density of 750,000 cells per well and harvested on the 7^{th} day after plating using RNABee (BioConnect, CS-104B) and RNA was extracted according to manufacturer's protocol.

Generation of forebrain neurons. For neuronal differentiation, NPCs at passage 6 were plated on to Matrigel-coated 6-well plates at a density of 200,000 cells per well in neural differentiation medium (DMEM/F12, N2, B27 without retinoic acid, 1µg/mL natural mouse laminin, 500µg/mL Dibutyryl cyclic-AMP, 20 ng/mL BDNF, 20ng/mL GDNF, 200nM L-Ascorbic Acid; [40]). Neurons were cultured for 4, 6 or 8 weeks with replacement of two thirds of the medium every 3 days. For immunostaining, additional neurons were plated on Matrigel-coated coverslips and similarly processed. At each neuronal time-point, immunohistostaining with MAP2 (Millipore MAB3418, 1:500) and Beta-3-Tubulin (Abcam ab18207, 1:1000) was performed for all samples to confirm their neuronal identity and cells for RNA sequencing were harvested using RNABee.

RNA was extracted using the same procedures as described for iNPC samples. Here, the term "iNeurons" refers to mixed forebrain neuron cultures.

RNA isolation, library preparation and sequencing. RNA samples were processed for RNA-sequencing to form two groups: 1) a larger discovery set; and 2) a smaller replication set. For the discovery set, 39 iNPC and 42 iNeuron RNA samples underwent RNA-sequencing. For the replication set, 21 iNeuron RNA samples collected at 6 weeks underwent RNA-sequencing. The integrity for each RNA sample was measured using the Agilent 2100 Bioanalyzer (Agilent, Santa Clara, CA, USA). All RNA integrity numbers (RINs) were greater than 8 (RIN: 9.59 $\pm$ 0.43). RNA samples were purified using PolyA selection, and the Illumina TruSeq Stranded Total RNA kit (Ilumina, San Diego, CA, USA) was used for library preparation, according to the manufacturer instructions. All indexed RNA libraries were pooled and sequenced using long read paired-end chemistry (2 $\times$ 150 bp) at an average read depth of ~50M reads per sample using the Illumina HiSeq2500. Resulting short reads with Illumina adapters were trimmed and low-quality reads were filtered using TrimGalore (*--illumina* option) [41]. All high-quality reads were then processed for alignment using the hg38 reference and the ultrafast universal RNA-seq aligner STAR (v2.5.1) [42] with default parameters. Mapped bam files were sorted using Samtools and short read data were quantified using featureCounts [43] with the following parameters: -T 5, -t exon, -g gene_id. Subsequently, all read counts were exported and all downstream analyses were performed in the R statistical computing environment.

RNA-seq data pre-processing and quality control. Raw count data was subjected to non-specific filtering to remove low-expressed genes that did not meet the requirement of a minimum of 2 counts per million (cpm) in at least ~40% of samples. This filtering threshold was applied to iNPC and iNeuron samples separately. All expression values were converted to $\log_2$ RPKM and

subjected to unsupervised principal component analysis (PCA) to identify and remove outlier samples that lay outside 95% confidence intervals from the grand averages as well as samples with aberrant X-inactivation gene expression profiles. A total of 32 iNPC and 42 iNeuron RNA-seq samples from the discovery set, and a total of 17 iNeuron samples from the replication set passed into downstream analyses.

Developmental specificity analysis. Two independent analyses were performed to confirm the developmental specificity of our iNPC and iNeuron gene expression data. First, we sought to confirm the developmental origin of our samples by integrating several RNA-seq data sets from post-mortem brain tissue and hiPSC models with our iNPC and iNeuron gene expression data using a previously described analytical approach [44]. A total of 15 independent studies were collected covering 2,716 independent samples and 11,650 genes. All expression values were converted to $\log_2$ RPKM and collectively normalized using quantile normalization from the *limma* R package [45]. These data, along with our iNPC and iNeuron expression data were analyzed jointly and integrated using principal component analysis (PCA). Second, we sought to confirm that highly expressed genes in our current data set are indeed preferentially prenatally biased in expression, based on BrainSpan developmental RNA-seq data. We previously applied a linear regression model to 299 neocortical BrainSpan samples ranging from 8 post-conceptual weeks to 40 years of age in order to characterize 22,141 genes as either prenatally or postnatally biased ($\log_2$FC > 0.1 and q < 0.05) or unbiased in expression (q > 0.05) [46]. The regression model generated a 'prenatal effect' (*t*-statistic) of the $\log_2$ fold-change of prenatal versus postnatal transcript abundance. We leveraged these summary statistics to examine the top 1000 most expressed and top 1000 least expressed genes in both iNPCs and iNeurons. Each gene set was examined to determine if the distribution of the fetal effect (*i.e.* t-statistics for each gene set)

differed significantly from the entire neocortical background using a Wilcoxon signed rank test. The neocortical background was defined as genes which were simultaneously detected by RNA-seq in the current study as well as genes found to be expressed in the neocortex following quality control procedures.

Cell type deconvolution analysis. The frequencies of neural cell types were estimated using Cibersort cell type deconvolution (https://cibersort.stanford.edu/) [47]. Cibersort relies on known cell subset specific marker genes to predict the proportions of cell types in heterogeneous bulk RNA-sequencing data. The method applies linear support vector regression, a machine learning approach that is robust compared to other methods with respect to noise, unknown mixture content and closely related cell types. As input, we used a reference panel of single-cell RNA-sequencing data from the human fetal cortex [48]. Cell specific gene signatures were curated using pre-defined cell clusters from the original publication covering four cell types: *i)* dividing intermediate progenitor cells (clusters 15-19); *ii)* excitatory neurons (clusters 21-28); *iii)* inhibitory neurons (clusters 38-46); and *iv)* mixed glial cells (clusters 4,6,9,19). Definitions for excitatory and inhibitory cell lineages in these data were defined in our previous work [46].

Quantifying transcriptome variance explained by known factors. Following data quality control, outlier detection and developmental specificity analysis (all described above), all gene expression values were normalized using VOOM normalization (a variance-stabilization transformation method) [45], and these data were used to carry out the remainder of downstream analyses. To understand the effects of various recorded factors on gene expression patterns, linear mixed effect models were applied to decompose the transcriptome variability into discrete percentages of variability attributable to multiple biological and technical sources of variation using the R package variancePartition [49]. For each gene, the percentage of gene expression

variation attributable to differences in cell types, individual as a repeated measure (*i.e.*, inter-donor effects), family effects, PMS diagnosis, RIN, age, biological sex, sequencing batch and variation in estimated cell type frequencies was computed. By properly attributing multiple sources of expression variation in this fashion, it is possible to identify and partially correct for some confounding variables in our differential gene expression analysis.

eQTL enrichment analysis. We used our previously described approach [44] to examine the overlap between genes with eQTLs from the CommonMind Consortium and genes exceeding a variance percentage cutoffs for a particular variable of interest in the current study. In brief, varianceParition analysis was applied to assign each gene a fraction of variance explained by a specific observed factor in the current analysis. A total of 40 different variance explained cutoff thresholds were examined and the overlap between genes with values exceeding this cutoff and the 2000 genes with the smallest *p*-values from cis-eQTL analysis is evaluated. The overlap is computed for the observed data and 10,000 data sets with the variance percentages randomly permutated. At each cutoff where > 100 genes are represented, the fold enrichment is computed as the observed overlap over the permuted overlap.

Differential gene expression analysis. Differential gene expression analyses were conducted using a moderated *t*-test from the R package limma [45]. All analyses adjusted for the possible confounding influence of biological sex, sequencing batch and RIN. Moreover, due to the repeated measures study design, where individuals are represented by multiple independent iNPC and iNeuron technical replicates, the duplicateCorrelation function was applied in the limma analysis and gene level significance values were adjusted for multiple testing using the Benjamini and Hochberg method to control the false discovery rate (FDR). Genes passing a FDR < 5% were labeled as showing significantly altered expression.

Functional enrichment of differentially expressed genes. Functional annotation was assessed in two complementary ways. First, all differentially expressed genes (FDR <5%) were functional annotated using the ToppFun module of ToppGene Suite software [50]. We explored Gene Ontology terms related to biological processes using a one-tailed hyper-geometric tested (Benjamini–Hochberg (BH) FDR corrected) to assess the significance of the overlap. Enrichment was examined separately for over-expressed and under-expressed genes. All terms must pass an FDR corrected *p*-value and a minimum of three genes per ontology were used as filters prior to pruning ontologies to less redundant terms. Second, we applied the camera function in the R package *limma* [45] to perform a competitive gene set test and to assess whether the genes in a given set are highly or lowly ranked in terms of differential gene expression relative to genes that are not in the set. The method leverages limma's linear model framework, taking both the design matrix and contrast matrix (if present) and accommodates the observational-level weights from *voom* in the testing procedure. After adjusting the variance of the resulting gene set test statistic by a variance inflation factor that depends on the gene-wise correlation (which is set to 0.01 by default) and the size of the set, a *p*-value is returned and adjusted for multiple testing.

Protein-protein interaction networks. The STRING database v11.0 [51] was used to assess whether differentially expressed genes were enriched for direct protein–protein interactions (PPIs) and to identify key genes mediating the regulation of multiple targets. For these analyses, our signature query of PMS-associated genes (FDR<5%) were used as input. STRING implements a scoring scheme to report the confidence level for each direct PPI (low confidence: < 0.4; medium: 0.4–0.7; high: > 0.7). We used a combined STRING score > 0.4. Hub genes within the PPI network are defined as those with the highest degree of network connections. We further used STRING to test whether the number of observed PPIs were significantly more than expected by chance using

a nontrivial random background model. For visualization, the STRING network was imported into Cytoscape [52].

CHD8 ChIP-Seq overlap analysis. To assess whether PMS-associated genes (FDR <5%) relate to known genome-wide CHD8 binding sites, we tested our differentially expressed gene sets for enrichment with human brain-specific sequences from two independent ChIP-seq studies covering: 1) 3,281 CHD8-binding sites in the human mid-fetal brain at 16-19 post-conception weeks [53]; and 2) 6,860 CHD8-binding sites in human neural progenitor cells [54] using the intersection of signal-enriched regions detected by all three CHD8 antibodies used in the study. In order to assess overlap with these binding sites, genomic coordinates were defined as the start and end positions for each differentially expressed gene (analogous to gene length). A permutation-based approach with 1,000 random permutations was used to determine statistical significance of the overlap between genomic coordinates for differentially expressed genes with CHD8-binding sites using the R package regioneR [55].

Weighted gene co-expression network analysis (WGCNA). Signed co-expression networks were built separately for iNPC and iNeuron samples using WGCNA [56]. To construct a global weighted network for each cell type, a total of 15,759 post QC genes across 32 iNPC samples and 16,721 genes across 42 iNeuron samples were used. The absolute values of Pearson's correlation coefficients were calculated for all possible gene pairs within each cell type and resulting values were transformed using a β-power (β=12 for iNPC samples; β=14 for iNeuron samples) so that the final correlation matrices followed an approximate scale-free topology. The WGCNA dynamic tree-cut algorithm was used to detect network modules (minimum module size =50; cut tree height = 0.99; deep-split = 2, merge module height = 0.20). Once network modules were identified, modules were assessed for significant associations to PMS diagnosis, as well as other biological

and technical factors. In order to determine which modules, and corresponding biological processes, were most associated with PMS, we ran singular value decomposition of each module's expression matrix and used the resulting module eigengene (ME), equivalent to the first principal component, to represent the overall expression profiles for each module. This technique is useful for reducing the number of multiple comparisons from thousands of genes to tens of modules. Gene co-expression modules that were significantly associated with PMS were subjected to functional annotation using the ToppFun module of ToppGene Suite software, as described above. Fisher's exact tests were used to assess the overlap of co-expression modules between iNPCs and iNeurons, while controlling FDR using the BH procedure.

Curation of autism and neurodevelopmental disorder gene sets. Two tiers of gene sets were collected to examine overlap with PMS-associated genes in the current study: (1) gene sets that implicate genetic risk for ASD and neurodevelopmental disorders (NDDs); and (2) gene sets that represent differentially expressed genes induced by knockdown (KD) or knockout (KO) of an ASD or NDD gene in iPSCs. For the gene sets that cover genetic evidence for ASD and NDDs we collected loci from: i) five lists of *de novo* variants implicated in ASD [46, 57-60]; ii) loci that implicate risk for intellectual disability (ID) [61, 62]; iii) genes implicated in developmental disorders (DD) from the DDG2P database [63]. We also included genes that are direct targets of FMRP [64]. For the gene sets from other iPSC transcriptome studies, we curated previously described differentially expressed genes caused by: *i)* shRNA KD of *SHANK3* in hiPSC-derived neurons [65]; *ii)* CRISPR/Cas9 heterozygous KO of *CHD8* in hiPSC-derived NPCs and neurons [66]; *iii)* shRNA KD of *TCF4* and *EHMT1* in hiPSC-derived NPCs [67]; *iv)* shRNA KD of *MBD5* and *SATB2* in human neural stem cells [68]; *v)* shRNA KD of *NRXN1* in human neural stem cells

[69]; and *vi)* CRISPR/Cas9 heterozygous and homozygous KO of ten different ASD-related genes in iPSCs and iPSC-derived neurons [70]. Full gene lists are provided in ***Supplemental Table 4***.

Gene overlap analyses. To compute significance of all gene-based overlaps, we used a the GeneOverlap function in R which uses a Fisher's Exact Test (FET) and an estimated odds-ratio for all pair-wise tests. Similarly, overrepresentation of ASD and NDD genetic risk gene sets within gene co-expression modules were analyzed a FET to assess the statistical significance. When testing overlap across gene modules, tests were adjusted for multiple testing using BH procedure to control the FDR.

Availability of data and materials. RNA-sequencing fastq files have been deposited in the Gene Expression Omnibus under accession number GSEXXXX (to be released following manuscript publication).

RESULTS

iNPC and iNeuron RNA-seq data generation and quality control

Peripheral blood samples were reprogrammed into hiPSCs and differentiated to generate iNPCs and iNeurons from a primary cohort of individuals with PMS (*n*=7; 2 males and 5 females) and their unaffected siblings (*n*=6; 3 males and 3 females; **Table 1**). The majority of the PMS probands studied here harbor subtelomeric deletions spanning 40-690 kbp, with the exception of one affected individual with a *SHANK3* point mutation. For all individuals, genome-wide RNA-sequencing was generated from iNPCs and from iNeurons at four, six and eight weeks in culture, to compare transcriptional differences between PMS probands and their unaffected siblings. For each participant, 1-to-3 clones were used for the NPC and neuronal induction yielding a total of 39 iNPC samples and 42 iNeuron samples in the discovery set (**Supplemental Table 1**).

372 Subsequently, all gene expression data were inspected for outlier samples on the basis of abnormal
373 gene expression profiles (*i.e.* samples beyond 95% confidence interval of grand mean), and six
374 iNPC samples were flagged and removed (**Figure S1A-B**). Next, because the extent of X-
375 inactivation in females has been reported to be a quality issue during iPSC reprogramming, we
376 examined the expression patterns of genes on the sex chromosomes using *XIST* on chrX and six
377 genes on chrY for all samples (**Figure S1C-D)**. This analysis identified six female iNPC samples
378 (five of which were already removed on the basis of outlier expression profiles) that have
379 expression patterns intermediate between males and females, consistent with either contamination
380 or aberrant X-inactivation, which were removed from our analysis.
381
382 **Developmental and cellular specificity of iNPCs and iNeurons**
383 We sought to determine whether our iNPC and iNeuron transcriptome data accurately reflects
384 early developmental gene expression profiles by integrating our RNA-seq data with other studies
385 using iPSC neuronal cell and post-mortem brain gene expression data. A total of 15 independent
386 studies were leveraged covering 11,650 genes and 2,719 developmentally distinct samples (*see*
387 *Materials and Methods*). Following standardized data pre-processing procedures, principal
388 component analysis (PCA) stratified all gene expression samples into a distinct developmental
389 axis starting with early embryonic stem cells and subsequently moving into iNPCs and iNeurons,
390 and into prenatal and postnatal postmortem brain samples (**Figure S2A**). Embryonic stem cells
391 (ESCs) and iPSCs clustered separately from iNPCs and iNeurons, which in turn co-clustered with
392 early prenatal brain samples. Notably, our iNPCs and iNeurons also co-cluster with iNPC and
393 iNeuron samples generated from previous reports confirming their early developmental gene
394 expression profiles. This clustering was robust to differing methodologies used for iPSC

395 reprogramming and differentiation across multiple prior studies. We also quantified whether the
396 genes with the highest expression in our iNPC and iNeuron data sets were predominantly
397 prenatally biased in expression using data from the BrainSpan project, and a clear prenatal bias in
398 expression was observed for genes with the highest levels of expression across both cell types
399 (**Figure S2B**). We also observed that genes with the lowest level of expression were predominantly
400 postnatally biased in expression, indicating that markers of later postnatal brain development are
401 expressed at low levels in the current data sets (**Figure S2C**).
402
403 It is possible that PMS-associated mutations could lead to unique neural cell type composition in
404 proband, as compared to sibling, cells. In addition, genetic background or stochastic factors may
405 also impact cell composition. We therefore estimated proportions of neural cell types for all iNPC
406 and iNeuron samples using a reference panel of single-cell RNA-sequencing data from the fetal
407 human cortex [48]. We observed that our iNPC samples were largely comprised of dividing
408 intermediate progenitor cells (~43.4%) and excitatory neurons (~23.1%), while iNeuron samples
409 were estimated to be comprised predominantly of excitatory neurons (~42.4%) and inhibitory
410 neurons (~24.8%) (**Figure S3**). Comparative analyses of the estimated cell type compositions
411 revealed minor increases in predicted proportions of excitatory neuron (p=0.04) and a decrease in
412 inhibitory neurons (p=0.002) in PMS probands relative to unaffected siblings (**Figure S3)**. These
413 *in silico* predictions suggest that differences in excitatory and inhibitory cell proportions may be
414 impacted by loss of *SHANK3*.
415
416 **Quantifying sources of gene expression variability: clinical, technical and biological factors**

Inter-donor and clonal variations have previously been reported to explain a substantial fraction of gene expression variability in iPSC-derived neural cells. Therefore, as a quality check, genome-wide concordance was evaluated between technical replicates, familial related and unrelated donors. Concordance between technical replicates was examined by either origin of the same clone and the same induction or the same clone but different induction (**Figure 1 A-B**). Our analysis confirmed that the strongest correlation was observed between technical replicates from the same clone and same induction followed by same clone and different induction in both iNPC and iNeuron samples. Subsequently, to test the influence of various factors on gene expression profiles, for each gene, the percentage of gene expression variation attributable to each clinical and technical factor was computed. Collectively, these variables explained ~55% of transcriptome variation, with differences between iNPC and iNeuron samples having the largest genome-wide effect that explained a median 29.2% of the observed variation, followed by differences in donor as a repeated measure (median 5.2%) and estimated excitatory cell type proportions (median 2.2%) (**Figure 1C**). The remaining factors explained smaller fractions of overall transcriptome variation, including family (median <0.1%) and biological sex (median <0.1%). Expression variation due to diagnosis (i.e., PMS proband) had a detectable effect in a smaller number of genes. Notably, when iNPC and iNeuron samples were analyzed separately, other technical variables such RNA integrity values, sequencing batch and total number of weeks in culture explained very little expression variation (**Figure S4**). Additionally, differences in *SHANK3* deletion size had a small but distinct effect on 50 genes, which were significantly overrepresented on chromosome 22 (**Figure S5A-B;** iNPCs, p=1.3e-31; iNeurons, p=3.2e-18). These genes were encompassed within the largest deletion reported here, and displayed clear patterns of under-expression relative to the other PMS probands (**Figure S5C**).

Next, the influence of cell type proportions, albeit predicted, were further evaluated by overlaying excitatory neuron cell type predictions on a PCA of the gene expression data. The PCA separated iNPCs and iNeurons along the first principal component (PC), explaining 86.4% of the variance, and excitatory neuron cell estimates were separated both by PC1 and PC2 (**Figure 1D**). As expected, iNeuron samples had a higher proportion of predicted excitatory neurons than iNPCs (mean increase = 19.3%, p = 1.97e-35 by linear model), and conversely iNPCs contain a higher proportion of predicted dividing intermediate neuron progenitor cells (mean increase = 23.7%, p =9.16=e-63 by linear model), consistent with results derived from our previous analyses. As a final measure, we took into account the recent observation that inter-donor variation in iNPCs and iNeurons reflects genetic regulation of gene expression and shows strong enrichment for expression quantitative trait loci (eQTLs). We tested this observation in our data and similarly confirmed that genes whose variance is largely explained by differences in donor are strongly enriched for eQTLs derived from post-mortem human brain samples (**Figure 1E**). Variation induced by differences in iNPC and iNeuron cells and predicted cell type proportions did not reflect such genetic differences between individuals and it is likely that either stochastic or epigenetic regulators could contribute to their variability.

Transcriptional signatures of PMS in iPSC-derived neural cells

Differential gene expression analyses comparing PMS probands and unaffected siblings identified 392 differentially expressed genes (DEGs) in iNPCs and 82 genes in iNeurons (FDR<5%; **Figure 2 A-B**, **Supplemental Table 2**), while adjusting for the possible influence of donor as a repeated measure, sex, RIN and sequencing batch. Genome-wide concordance was examined between

463 iNPCs and iNeurons using PMS-associated $\log_2$ fold-changes, and a remarkably similar patterns
464 of differential gene expression were observed between PMS probands and unaffected siblings in
465 both cell types (**Figure 2C**; R=0.43, p <2.2e-16). Moreover, nine statistically significant DEGs
466 were detected across both iNPCs and iNeurons, and each displayed the same direction of effect in
467 PMS, including three genes which were consistently over-expressed (*ARHGAP20*, *PCYT2*,
468 *CAMK2N1*) and six genes which were consistently under-expressed in PMS (*SHANK3*, *PSMD5-*
469 *AS1*, *GPC3*, *TSHZ2*, *RP11-655M14.13 (lincRNA)*, *RP11-115D19.1 (lcRNA)*). Functional
470 annotation of DEGs revealed strong pathway and biological enrichment for genes that were
471 predominantly under-expressed in PMS in both iNPCs and iNeurons covering several early
472 developmental terms and pathways, including 20 genes mapping to the Wnt signaling pathway
473 (*e.g. FRZB, G3BP1, GPC3, GPC6, MLLT3, ROR2, RSPO3, WNT3A, WNT4*) (**Figure 2D**). Several
474 biological processes were uniquely enriched among the under-expressed genes in iNeurons,
475 including extracellular matrix (ECM)-related process, protein translation-related terms (*e.g,*.
476 peptide chain elongation, translational termination/elongation/regulation/initiation) and nonsense
477 mediated decay (**Figure 2E**). Overexpressed genes in iNeurons also displayed enrichment for
478 genes involved in pre- and post-synaptic activity, cholesterol biosynthesis, transmission across
479 chemical synapses, GABAergic synapses, G protein gated-potassium channels, signaling by
480 insulin receptor, signaling to ERKs, glutamate binding and activation of AMPA receptors (**Figure**
481 **2F**). No enrichment was observed for over-expressed genes in PMS iNPC samples. Notably,
482 adjusting for differing cell type proportions within iNPC and iNeuron samples had little effect on
483 the resulting differential gene expression signatures (**Figure S6; Table S2**). A full table of
484 enrichment terms can be found in *Supplemental Table 3*.
485

To support these functional enrichment observations, we tested whether candidate genes that are dysregulated together indeed interact with each other at the protein level. A significant overrepresentation of direct protein-protein interactions (PPI) was identified for differentially expressed genes in iNPCs (p=2.32e-09, average node degree=1.81) and iNeurons (p= 4.19e-09, average node degree=0.81). In iNPC, hub genes in the PPI included genes involved in glutamate receptor signaling pathway, including *GRM3*, *GRIA1*, *CAMK2A* and several homeobox genes (**Figure S7A**). The iNeuron PPI network was notably smaller in edges and nodes, and components of the Wnt signaling pathway emerged as candidate hub genes, including *WNT3A*, *WNT7B* and *FRZB* (**Figure S7B**). Given that many of these genes share similar functions and interactions, we queried whether these transcriptional signatures also shared common brain-specific regulatory mechanisms. To this end, we related DEGs in PMS to well-curated binding sites for *CHD8*, a chromodomain helicase strongly associated with ASD, using *CHD8* ChIP-sequencing data from two independent studies. Among DEGs in iNPCs, significant enrichment was observed for *CHD8* binding sites derived from the human mid-fetal brain (p=0.03) and for binding sites derived from human NPCs (p=0.001). No significant enrichment for *CHD8* binding sites was observed for DEGs in iNeurons (p=0.46, p=0.41, respectively; **Figure S8**).

Co-expression modules associated with PMS

Given that the majority of the PMS-associated genes share similar functions and interactions, we tested whether these genes are also co-expressed. We applied unsupervised WGCNA separately to iNPCs and iNeurons to identify small sets of genes with similar co-expression patterns. A total of 19 co-expression modules were identified in NPCs and 22 modules were identified in iNeuron samples, and all modules were well preserved between iNPCs and iNeurons (**Figure S9**). Each

509 module was assessed for overrepresentation of differentially expressed genes in PMS as well as
510 previously reported genetic risk loci for ASD and other NDDs (**Figure 3A**). Genes that were
511 differentially expressed in PMS iNPCs were significantly overrepresented in iNPC module M4
512 (∩=53, p=1.53e-41), while differentially expressed genes in iNeurons were strongly enriched
513 across three iNeuron modules: M2 (∩=12, p=0.003), M4 (∩=14, p=2.6e-5) and M19 (∩=32,
514 p=2.15e-21). Notably, module M2 in iNeurons harbored a significant fraction of genetic risk loci
515 for ID (∩=5, p=0.02), while module M4 in iNeurons was enriched for DD (∩=14, p=0.02) and ID
516 (∩=5, p=0.002) risk loci. Module eigengene (ME) values for all modules were then regressed onto
517 individual diagnostic status (*i.e.* PMS probands), which confirmed significant module-trait
518 associations for module M4 in iNPCs with PMS (r=-0.58, p=6e-04) as well as iNeuron modules
519 M2 (r=0.50, p=9e-04), M4 (r=0.55, p=2e-04) and M19 (r=-0.55, p=2e-04) with PMS (**Figure 3B**).
520 Next, the gene-module assignments identified for iNPC and iNeuron samples, respectively, were
521 used to perform supervised module construction for the same set of genes in the contrasting cell
522 type (*i.e.* genes in module M1 identified in iNPCs were forced to form a module in iNeurons),
523 which were similarly tested for association with PMS. In doing so, we found that genes that were
524 either negatively or positively associated with PMS in one cell type, displayed similar levels of
525 association to PMS in the other cell type (**Figure 3B**), consistent with our differential gene
526 expression analysis (**Figure 2C**). Functional annotation of these candidate modules revealed
527 similar biological functions as previously reported from differential gene expression, including
528 under-expression of iNPC module M4 and iNeuron module, which were both enriched for early
529 embryonic development gene sets, ECM, neurogenesis and Wnt signaling (**Figure 3C**). In
530 iNeurons, module M2 was positively associated with PMS and was implicated in GDP binding,
531 response to oxygen/stress/hormones, LRR domain binding. A separate iNeuron module M4 was

532 enriched for GTPase signaling, postsynaptic signal transduction and axon guidance-related
533 processes.
534
535 **Overlap with existing ASD transcriptome iPSC reports**
536 We also explored points of convergence between our *SHANK3*-deficiency findings in PMS with
537 gene expression changes induced by either shRNA knockdown (KD) or CRISPR/Cas9 knockout
538 (KO) of other top ranked ASD genes assayed in neural cell types (**Table 2; Figure S10**). A total
539 of 6 iPSC transcriptome studies spanning 17 different ASD and NDD genes were evaluated. We
540 identified several significant overlaps between PMS-associated gene findings in both iNPCs and
541 iNeurons with gene expression perturbations associated with: *i) SHANK3* KD in neurons (∩=20,
542 FET=2.4e-7; ∩=44, FET=0.003, respectively); *ii) CHD8* KO in NPCs (∩=33, FET=0.004; ∩=15,
543 FET=0.1.8e-5, respectively); *iii) CHD8* KO in neurons (∩=91, FET=1.3e-7; ∩=29, FET=5.7e-7,
544 respectively); *iv) EHMT1* KD in NPCs (∩=23, FET=0.001; ∩=10, FET=0.001, respectively); *v)*
545 *NRXN1* KD in stem cells (∩=8, FET=0.001; ∩=4, FET=0.04, respectively); *vi) SCN2A* KO in
546 iPSCs (∩=55, p=0.0002; ∩=16, p=0.001, respectively); *vii) ATRX* KO in iPSCs (∩=32, FET=0.03;
547 ∩=10, FET=0.02, respectively); and *viii) ATRX* KO in neurons (∩=47, FET=6.73e-7; ∩=12,
548 FET=0.002, respectively). In addition, differentially expressed genes in PMS iNeurons, but not in
549 iNPCs, were enriched for genes associated with: *ix) SATB2* KD in stem cells (∩=8, FET=0.0002);
550 and *x) TNEM1* KO in neurons (∩=7, p=0.004). Importantly, the vast majority of these observed
551 overlaps were consistently enriched for genes implicating changes in Wnt signaling, ECM,
552 perineuronal net and glutamatergic synapses (**Table 2; Figure S10**).
553
554 **Validation of PMS-associated gene dysregulation in iNeurons**

555 To validate our PMS transcriptional signatures, we performed additional RNA-sequencing on a
556 replication set of 21 iNeurons collected at 6 weeks. Following data preprocessing, four samples
557 were removed on the basis of aberrant X-inactivation (**Figure S11A-B**) and a total of eight
558 biological replicates derived from independent differentiations and nine technical replicates passed
559 into our subsequent validation analyses. *In silico* predictions of cell type frequencies validated the
560 trending decreases in inhibitory neurons (p=0.05) and increases in excitatory neurons (p=0.08),
561 albeit to an insignificant extent in PMS (**Figure S11C**). Subsequently, sample-to-sample
562 correlation coefficients were evaluated between discovery and replication samples, first among
563 technical replicates (median R=0.98), then among biological replicates derived from independent
564 differentiations (median R=0.96) and between unrelated donors (median R=0.94) (**Figure 4A**).
565 Overall, levels of concordance were highest between technical replicates relative to those observed
566 between biological replicates (p=2.6e-9) and unrelated donors (p=7.7e-12). Next, differentially
567 expressed genes were computed using the replication set of iNeurons and genome-wide
568 concordance of PMS-associated $\log_2$ fold-changes were regressed onto $\log_2$ fold-changes
569 computed using different combinations of discovery set iNeuron samples: i) six week samples; ii)
570 four and eight week samples; or iii) four, six and eight week samples. As expected, the highest
571 levels of concordance were observed between discovery and replication six week samples
572 (R=0.92) followed by a combination of four, six and eight weeks (R=0.86) and subsequently four
573 and eight week samples (R=0.80) (**Figure 4B**).
574
575

DISCUSSION

Our study sought to characterize transcriptional signatures of *SHANK3* haploinsufficiency in neurodevelopment, by comparing genome-wide RNA-seq profiles of iNPCs and iNeurons derived from individuals with PMS with those of their unaffected siblings. We report on the largest sample set of PMS-derived iNPCs and iNeurons to date, representative of a range of genetic lesions associated with PMS, from a *SHANK3* point mutation to small and large 22q13.3 deletions. DEGs in our dataset were enriched for pathways involved in core developmental processes such as pattern specification and embryonic morphogenesis, including Wnt signaling pathways that are essential for neuronal fate specification. Gene co-expression modules generated from these data demonstrated convergence between altered PMS molecular pathways and ASD and NDD genetic risk loci. Importantly, overlapping DEG findings were identified between the current study and findings from other ASD and NDD transcriptome iPSC studies, demonstrating overlapping changes in RNA involved in Wnt signaling, ECM and glutamatergic synapses.

The transcriptional signatures of PMS in iNeurons point to altered postsynaptic density, glutamatergic synaptic and GABAergic genes. Our results are in line with evidence supporting a role for *SHANK3* prior to synaptogenesis and neural circuit formation, specifically in early morphogenesis and excitatory/ inhibitory balance [32, 65, 71-74]. For example, a zebrafish model of PMS that utilized morpholinos to disrupt shank3a and shank3b resulted in delayed mid- and hindbrain development, disruptions in motor behaviors, and seizure-like behaviors [73].

SHANK3 may mediate presynaptic function via transynaptic signaling through cell adhesion molecules such as neurexin and neuroligin [75, 76]. In a rat hippocampal *in vitro* model, *SHANK3*

599 expression was found to affect transynaptic signaling by modulating pre- and postsynaptic protein
600 content and neurotransmission efficiency through neurexin-neuroligin interactions [74]. *SHANK3*
601 has been shown to bind neuroligin via its PDZ domain [77], therefore potentially regulating
602 synaptic strength via retrograde signaling through cell adhesion molecules. In addition, since
603 neurexin-neuroligin are implicated in the regulation and coordination of synaptic function via
604 transynaptic signaling [76], with some evidence of NMDAR regulation involvement [78], their
605 association with *SHANK3* presents with one possible mechanism by which *SHANK3* disruption
606 could dysregulate excitatory/inhibitory balance in the developing brain.
607
608 Our group has previously shown that *SHANK3* point mutations are sufficient to convey a PMS
609 phenotype [4], although larger deletion sizes have been associated with a more severe range of
610 PMS manifestations [6, 7, 41]. Here, we find that differences in *SHANK3* deletion size have a
611 significant dosage effect on 50 genes that span the largest deletion in our dataset. One of these
612 genes, *WNT7B*, had been previously associated with macrocephaly and chromosome 22 deletions
613 greater than 5Mb [7]. *WNT7B* codes for a secreted signaling protein that is central to Wnt signaling
614 pathway, which is also enriched in our dataset and has been implicated in *SHANK3* deficiency in
615 previous reports [79]. These findings suggest that genes in close proximity to *SHANK3* on
616 chromosome 22 may also play a role in modulating the pathobiology of PMS.
617
618 We also found several points of convergence on ECM and Wnt signaling in PMS and other iPSC
619 studies of ASD and NDDs. Numerous lines of evidence point to Wnt signaling as a candidate
620 pathway implicated in ASD etiology [80]. In previous reports, mutations of Wnt signaling pathway
621 genes involved in processes such as neurite growth, synapse formation, neurogenesis and

622 corticogenesis have been associated with ASD phenotypes [81, 82]. For example, *CTNNB1,* which
623 produces the protein β-catenin, plays a critical role in cell adhesion and cell signaling in the Wnt
624 signaling pathway and *de novo* mutations in *CTNNB1* have been linked to individuals with DD,
625 ID and ASD [46]. In murine models, stabilization of *CTNNB1* in cortical samples has been found
626 to increase Wnt signaling and boost neurogenesis [83], while depletion of *CTNNB1* from inhibitory
627 neurons leads to deficits in neuronal activation and ASD-like behavior [84]. Numerous top-ranked
628 ASD risk genes have also been found to function with *CTNNB1* and the Wnt signaling pathway.
629 For example, *CHD8* is a chromatin remodeling factor and a top-ranked ASD risk gene, which has
630 been shown to be a positive regulator of *CTNNB1*-mediated Wnt signaling in NPCs [85]. Notably,
631 many under-expressed genes in the current dataset show enrichment for both Wnt signaling genes
632 and *CHD8* binding sites. Both *PTEN* and *TCF7L2* also represent ASD and ID risk genes [58, 60,
633 86, 87], respectively, and have been identified to function with *CTNNB1* to regulate normal brain
634 growth [88] and to initiate transcriptional responses following Wnt receptor binding [89].
635 Additionally, *de novo* mutations in *DDX3X* are associated with ID and ASD [90], and this gene
636 has been recently identified to be an important component of *CTNNB1*-mediated Wnt signaling by
637 regulating kinase activity, which in turn promote phosphorylation of Dvl and represents a major
638 hub in the Wnt pathway [91]. Therefore, in addition to ASD, *CTNNB1*-mediated Wnt signaling
639 may be disrupted in ID and other NDDs, further underscoring the points of convergence identified
640 the current study and demonstrating the importance of this pathway in proper neurodevelopment.
641
642 Given the described changes in the Wnt signaling pathway, a follow-up question would be whether
643 pharmacological regulation of Wnt signaling represents an important and/or plausible treatment
644 strategy for PMS and ASD. Notably, several medications have been shown to modulate Wnt
645 signaling, including methylphenidates [92], selective serotonin reuptake inhibitors (SSRIs) [93]

and some antipsychotic medications [89, 94]. For example, long-term administration of methylphenidate in mice has been shown to modulate key components of the Wnt signaling pathway, including Akt and GSK3 [92]. Similarly, SSRI treatment (*e.g.* fluoxetine) has been shown to boost Wnt signaling, specifically *Wnt2* and *Wnt3* in two different mouse studies [93, 95]. Further, two additional reports have also demonstrated that the antipsychotic medication haloperidol promotes Wnt signalling, including *WNT5A* and β-catenin expression [96] as well as the phosphorylation of Akt [94]. Overall, it is noteworthy that several pharmacological interventions for behavioral disorders affect components of Wnt signaling, either directly or indirectly. However, additional investigations are required to determine the role of these mechanisms and compare the treatment efficacy across individuals with and without Wnt signaling abnormalities.

The current study also presents some limitations. First, given the rarity of PMS, we could not carry out experimental validation in independent biological samples. Nevertheless, in an effort to boost signal over noise, several points of convergence were identified with gene-based findings from other iPSC transcriptome studies. Second, loss of *SHANK3* has been shown to affect neurite length, complexity of neurite arborization and soma area, which were not examined in the current study and may contribute to some of the observed transcriptional changes. Third, while *in silico* predictions of cell type proportions attempted to control and quantify the variance in these transcriptome data, it remains possible that some transcriptional changes can be related to changes in proportions of specific cell types. This is especially true when studying iNeurons, which reflect a heterogeneous mixture of neuronal subpopulations and mixed glial cells. Single-cell RNA-

668 sequencing of iNeurons at different differentiation stages may produce a clearer picture of the
669 underlying cellular heterogeneity and corresponding gene expression profiles in such samples.

670

671 In summary, our study demonstrates that *SHANK3*-deficiency results in profound transcriptional
672 changes in PMS-derived hiPSC-iNPCs and hiPSC-iNeurons. Many early developmental pathways
673 are impacted, including altered processes related to pre-and post-synaptic signaling, embryonic
674 development and function, as well as Wnt and ECM signaling. Several other iPSC transcriptome
675 studies of ASD and NDD genes also displayed changes in ECM and Wnt signaling, providing
676 molecular insights into PMS and into NDDs more broadly.

677

678 **REFERENCES**

679 1. Betancur C, Buxbaum JD: **SHANK3 haploinsufficiency: a "common" but underdiagnosed**
680 **highly penetrant monogenic cause of autism spectrum disorders**. *Mol Autism* 2013, **4**(1):17.
681 2. Leblond CS, Nava C, Polge A, Gauthier J, Huguet G, Lumbroso S, Giuliano F, Stordeur C,
682 Depienne C, Mouzat K *et al*: **Meta-analysis of SHANK Mutations in Autism Spectrum**
683 **Disorders: a gradient of severity in cognitive impairments**. *PLoS Genet* 2014, **10**(9):e1004580.
684 3. Boccuto L, Lauri M, Sarasua SM, Skinner CD, Buccella D, Dwivedi A, Orteschi D, Collins JS,
685 Zollino M, Visconti P *et al*: **Prevalence of SHANK3 variants in patients with different subtypes**
686 **of autism spectrum disorders**. *Eur J Hum Genet* 2013, **21**(3):310-316.
687 4. De Rubeis S, Siper PM, Durkin A, Weissman J, Muratet F, Halpern D, Trelles MDP, Frank Y,
688 Lozano R, Wang AT *et al*: **Delineation of the genetic and clinical spectrum of Phelan-**
689 **McDermid syndrome caused by SHANK3 point mutations**. *Mol Autism* 2018, **9**:31.

5. Mitz AR, Philyaw TJ, Boccuto L, Shcheglovitov A, Sarasua SM, Kaufmann WE, Thurm A: **Identification of 22q13 genes most likely to contribute to Phelan McDermid syndrome**. *Eur J Hum Genet* 2018, **26**(3):293-302.

6. Soorya L, Kolevzon A, Zweifach J, Lim T, Dobry Y, Schwartz L, Frank Y, Wang AT, Cai G, Parkhomenko E *et al*: **Prospective investigation of autism and genotype-phenotype correlations in 22q13 deletion syndrome and SHANK3 deficiency**. *Mol Autism* 2013, **4**(1):18.

7. Sarasua SM, Dwivedi A, Boccuto L, Chen CF, Sharp JL, Rollins JD, Collins JS, Rogers RC, Phelan K, DuPont BR: **22q13.2q13.32 genomic regions associated with severity of speech delay, developmental delay, and physical features in Phelan-McDermid syndrome**. *Genet Med* 2014, **16**(4):318-328.

8. Durand CM, Perroy J, Loll F, Perrais D, Fagni L, Bourgeron T, Montcouquiol M, Sans N: **SHANK3 mutations identified in autism lead to modification of dendritic spine morphology via an actin-dependent mechanism**. *Mol Psychiatry* 2012, **17**(1):71-84.

9. Halbedl S, Schoen M, Feiler MS, Boeckers TM, Schmeisser MJ: **Shank3 is localized in axons and presynaptic specializations of developing hippocampal neurons and involved in the modulation of NMDA receptor levels at axon terminals**. *J Neurochem* 2016, **137**(1):26-32.

10. Monteiro P, Feng G: **SHANK proteins: roles at the synapse and in autism spectrum disorder**. *Nat Rev Neurosci* 2017, **18**(3):147-157.

11. Lee K, Vyas Y, Garner CC, Montgomery JM: **Autism-associated Shank3 mutations alter mGluR expression and mGluR-dependent but not NMDA receptor-dependent long-term depression**. *Synapse* 2019, **73**(8):e22097.

12. Ponna SK, Ruskamo S, Myllykoski M, Keller C, Boeckers TM, Kursula P: **Structural basis for PDZ domain interactions in the post-synaptic density scaffolding protein Shank3**. *J Neurochem* 2018, **145**(6):449-463.

13. Shi R, Redman P, Ghose D, Hwang H, Liu Y, Ren X, Ding LJ, Liu M, Jones KJ, Xu W: **Shank Proteins Differentially Regulate Synaptic Transmission**. *eNeuro* 2017, **4**(6).

14. Verpelli C, Dvoretskova E, Vicidomini C, Rossi F, Chiappalone M, Schoen M, Di Stefano B, Mantegazza R, Broccoli V, Bockers TM *et al*: **Importance of Shank3 protein in regulating metabotropic glutamate receptor 5 (mGluR5) expression and signaling at synapses**. *J Biol Chem* 2011, **286**(40):34839-34850.

15. Bey AL, Wang X, Yan H, Kim N, Passman RL, Yang Y, Cao X, Towers AJ, Hulbert SW, Duffney LJ *et al*: **Brain region-specific disruption of Shank3 in mice reveals a dissociation for cortical and striatal circuits in autism-related behaviors**. *Transl Psychiatry* 2018, **8**(1):94.

16. Bozdagi O, Sakurai T, Papapetrou D, Wang X, Dickstein DL, Takahashi N, Kajiwara Y, Yang M, Katz AM, Scattoni ML *et al*: **Haploinsufficiency of the autism-associated Shank3 gene leads to deficits in synaptic function, social interaction, and social communication**. *Mol Autism* 2010, **1**(1):15.

17. Dhamne SC, Silverman JL, Super CE, Lammers SHT, Hameed MQ, Modi ME, Copping NA, Pride MC, Smith DG, Rotenberg A *et al*: **Replicable in vivo physiological and behavioral phenotypes of the Shank3B null mutant mouse model of autism**. *Mol Autism* 2017, **8**:26.

18. Drapeau E, Riad M, Kajiwara Y, Buxbaum JD: **Behavioral Phenotyping of an Improved Mouse Model of Phelan-McDermid Syndrome with a Complete Deletion of the Shank3 Gene**. *eNeuro* 2018, **5**(3).

19. Ferhat AT, Halbedl S, Schmeisser MJ, Kas MJ, Bourgeron T, Ey E: **Behavioural Phenotypes and Neural Circuit Dysfunctions in Mouse Models of Autism Spectrum Disorder**. *Adv Anat Embryol Cell Biol* 2017, **224**:85-101.

20. Jaramillo TC, Speed HE, Xuan Z, Reimers JM, Liu S, Powell CM: **Altered Striatal Synaptic Function and Abnormal Behaviour in Shank3 Exon4-9 Deletion Mouse Model of Autism**. *Autism Res* 2016, **9**(3):350-375.

21. Kouser M, Speed HE, Dewey CM, Reimers JM, Widman AJ, Gupta N, Liu S, Jaramillo TC, Bangash M, Xiao B *et al*: **Loss of predominant Shank3 isoforms results in hippocampus-**

dependent impairments in behavior and synaptic transmission. *J Neurosci* 2013, **33**(47):18448-18468.

22. Lee J, Chung C, Ha S, Lee D, Kim DY, Kim H, Kim E: **Shank3-mutant mice lacking exon 9 show altered excitation/inhibition balance, enhanced rearing, and spatial memory deficit**. *Front Cell Neurosci* 2015, **9**:94.

23. Peca J, Feliciano C, Ting JT, Wang W, Wells MF, Venkatraman TN, Lascola CD, Fu Z, Feng G: **Shank3 mutant mice display autistic-like behaviours and striatal dysfunction**. *Nature* 2011, **472**(7344):437-442.

24. Speed HE, Kouser M, Xuan Z, Reimers JM, Ochoa CF, Gupta N, Liu S, Powell CM: **Autism-Associated Insertion Mutation (InsG) of Shank3 Exon 21 Causes Impaired Synaptic Transmission and Behavioral Deficits**. *J Neurosci* 2015, **35**(26):9648-9665.

25. Wang X, Bey AL, Katz BM, Badea A, Kim N, David LK, Duffney LJ, Kumar S, Mague SD, Hulbert SW *et al*: **Altered mGluR5-Homer scaffolds and corticostriatal connectivity in a Shank3 complete knockout model of autism**. *Nat Commun* 2016, **7**:11459.

26. Wang X, McCoy PA, Rodriguiz RM, Pan Y, Je HS, Roberts AC, Kim CJ, Berrios J, Colvin JS, Bousquet-Moore D *et al*: **Synaptic dysfunction and abnormal behaviors in mice lacking major isoforms of Shank3**. *Hum Mol Genet* 2011, **20**(15):3093-3108.

27. Harony-Nicolas H, Kay M, du Hoffmann J, Klein ME, Bozdagi-Gunal O, Riad M, Daskalakis NP, Sonar S, Castillo PE, Hof PR *et al*: **Oxytocin improves behavioral and electrophysiological deficits in a novel Shank3-deficient rat**. *Elife* 2017, **6**.

28. Berg EL, Copping NA, Rivera JK, Pride MC, Careaga M, Bauman MD, Berman RF, Lein PJ, Harony-Nicolas H, Buxbaum JD *et al*: **Developmental social communication deficits in the Shank3 rat model of phelan-mcdermid syndrome and autism spectrum disorder**. *Autism Res* 2018, **11**(4):587-601.

765 29. Mokhtari R, Lachman HM: **Neurons Derived From Patient-Specific Induced Pluripotent Stem**
766 **Cells: a Promising Strategy Towards Developing Novel Pharmacotherapies for Autism**
767 **Spectrum Disorders**. *EBioMedicine* 2016, **9**:21-22.
768 30. Shen X, Yeung HT, Lai KO: **Application of Human-Induced Pluripotent Stem Cells (hiPSCs)**
769 **to Study Synaptopathy of Neurodevelopmental Disorders**. *Dev Neurobiol* 2019, **79**(1):20-35.
770 31. Shcheglovitov A, Shcheglovitova O, Yazawa M, Portmann T, Shu R, Sebastiano V, Krawisz A,
771 Froehlich W, Bernstein JA, Hallmayer JF *et al*: **SHANK3 and IGF1 restore synaptic deficits in**
772 **neurons from 22q13 deletion syndrome patients**. *Nature* 2013, **503**(7475):267-271.
773 32. Kathuria A, Nowosiad P, Jagasia R, Aigner S, Taylor RD, Andreae LC, Gatford NJF, Lucchesi W,
774 Srivastava DP, Price J: **Stem cell-derived neurons from autistic individuals with SHANK3**
775 **mutation show morphogenetic abnormalities during early development**. *Mol Psychiatry* 2018,
776 **23**(3):735-746.
777 33. Gouder L, Vitrac A, Goubran-Botros H, Danckaert A, Tinevez JY, Andre-Leroux G, Atanasova E,
778 Lemiere N, Biton A, Leblond CS *et al*: **Altered spinogenesis in iPSC-derived cortical neurons**
779 **from patients with autism carrying de novo SHANK3 mutations**. *Sci Rep* 2019, **9**(1):94.
780 34. Darville H, Poulet A, Rodet-Amsellem F, Chatrousse L, Pernelle J, Boissart C, Heron D, Nava C,
781 Perrier A, Jarrige M *et al*: **Human Pluripotent Stem Cell-derived Cortical Neurons for High**
782 **Throughput Medication Screening in Autism: A Proof of Concept Study in SHANK3**
783 **Haploinsufficiency Syndrome**. *EBioMedicine* 2016, **9**:293-305.
784 35. Bidinosti M, Botta P, Kruttner S, Proenca CC, Stoehr N, Bernhard M, Fruh I, Mueller M, Bonenfant
785 D, Voshol H *et al*: **CLK2 inhibition ameliorates autistic features associated with SHANK3**
786 **deficiency**. *Science* 2016, **351**(6278):1199-1203.
787 36. Vicidomini C, Ponzoni L, Lim D, Schmeisser MJ, Reim D, Morello N, Orellana D, Tozzi A,
788 Durante V, Scalmani P *et al*: **Homer1b/c clustering is impaired in Phelan-McDermid Syndrome**
789 **iPSCs derived neurons**. *Mol Psychiatry* 2017, **22**(5):637.

37. Yi F, Danko T, Botelho SC, Patzke C, Pak C, Wernig M, Sudhof TC: **Autism-associated SHANK3 haploinsufficiency causes Ih channelopathy in human neurons**. *Science* 2016, **352**(6286):aaf2669.

38. Yang W, Mills JA, Sullivan S, Liu Y, French DL, Gadue P: **iPSC Reprogramming from Human Peripheral Blood Using Sendai Virus Mediated Gene Transfer**. In: *StemBook*. Cambridge (MA); 2008.

39. Bock C, Kiskinis E, Verstappen G, Gu H, Boulting G, Smith ZD, Ziller M, Croft GF, Amoroso MW, Oakley DH *et al*: **Reference Maps of human ES and iPS cell variation enable high-throughput characterization of pluripotent cell lines**. *Cell* 2011, **144**(3):439-452.

40. Brennand KJ, Simone A, Jou J, Gelboin-Burkhart C, Tran N, Sangar S, Li Y, Mu Y, Chen G, Yu D *et al*: **Modelling schizophrenia using human induced pluripotent stem cells**. *Nature* 2011, **473**(7346):221-225.

41. Bolger AM, Lohse M, Usadel B: **Trimmomatic: a flexible trimmer for Illumina sequence data**. *Bioinformatics* 2014, **30**(15):2114-2120.

42. Dobin A, Davis CA, Schlesinger F, Drenkow J, Zaleski C, Jha S, Batut P, Chaisson M, Gingeras TR: **STAR: ultrafast universal RNA-seq aligner**. *Bioinformatics* 2013, **29**(1):15-21.

43. Liao Y, Smyth GK, Shi W: **featureCounts: an efficient general purpose program for assigning sequence reads to genomic features**. *Bioinformatics* 2014, **30**(7):923-930.

44. Hoffman GE, Hartley BJ, Flaherty E, Ladran I, Gochman P, Ruderfer DM, Stahl EA, Rapoport J, Sklar P, Brennand KJ: **Transcriptional signatures of schizophrenia in hiPSC-derived NPCs and neurons are concordant with post-mortem adult brains**. *Nat Commun* 2017, **8**(1):2225.

45. Ritchie ME, Phipson B, Wu D, Hu Y, Law CW, Shi W, Smyth GK: **limma powers differential expression analyses for RNA-sequencing and microarray studies**. *Nucleic Acids Res* 2015, **43**(7):e47.

46. Satterstrom FK, Kosmicki J, Wang J, Breen MS, De Rubeis S, An JY, Peng M, Collins R, Grove J, Klei L *et al*: **Large-scale exome sequencing study implicates both developmental and**

functional changes in the neurobiology of autism. *bioRxiv* 2019, **484113**(doi: https://doi.org/10.1101/484113).

47. Newman AM, Liu CL, Green MR, Gentles AJ, Feng W, Xu Y, Hoang CD, Diehn M, Alizadeh AA: **Robust enumeration of cell subsets from tissue expression profiles**. *Nat Methods* 2015, **12**(5):453-457.

48. Nowakowski TJ, Bhaduri A, Pollen AA, Alvarado B, Mostajo-Radji MA, Di Lullo E, Haeussler M, Sandoval-Espinosa C, Liu SJ, Velmeshev D *et al*: **Spatiotemporal gene expression trajectories reveal developmental hierarchies of the human cortex**. *Science* 2017, **358**(6368):1318-1323.

49. Hoffman GE, Schadt EE: **variancePartition: interpreting drivers of variation in complex gene expression studies**. *BMC Bioinformatics* 2016, **17**(1):483.

50. Chen J, Bardes EE, Aronow BJ, Jegga AG: **ToppGene Suite for gene list enrichment analysis and candidate gene prioritization**. *Nucleic Acids Res* 2009, **37**(Web Server issue):W305-311.

51. Szklarczyk D, Gable AL, Lyon D, Junge A, Wyder S, Huerta-Cepas J, Simonovic M, Doncheva NT, Morris JH, Bork P *et al*: **STRING v11: protein-protein association networks with increased coverage, supporting functional discovery in genome-wide experimental datasets**. *Nucleic Acids Res* 2019, **47**(D1):D607-D613.

52. Shannon P, Markiel A, Ozier O, Baliga NS, Wang JT, Ramage D, Amin N, Schwikowski B, Ideker T: **Cytoscape: a software environment for integrated models of biomolecular interaction networks**. *Genome Res* 2003, **13**(11):2498-2504.

53. Cotney J, Muhle RA, Sanders SJ, Liu L, Willsey AJ, Niu W, Liu W, Klei L, Lei J, Yin J *et al*: **The autism-associated chromatin modifier CHD8 regulates other autism risk genes during human neurodevelopment**. *Nat Commun* 2015, **6**:6404.

54. Sugathan A, Biagioli M, Golzio C, Erdin S, Blumenthal I, Manavalan P, Ragavendran A, Brand H, Lucente D, Miles J *et al*: **CHD8 regulates neurodevelopmental pathways associated with**

autism spectrum disorder in neural progenitors. *Proc Natl Acad Sci U S A* 2014, **111**(42):E4468-4477.

55. Gel B, Diez-Villanueva A, Serra E, Buschbeck M, Peinado MA, Malinverni R: **regioneR: an R/Bioconductor package for the association analysis of genomic regions based on permutation tests**. *Bioinformatics* 2016, **32**(2):289-291.

56. Langfelder P, Horvath S: **WGCNA: an R package for weighted correlation network analysis**. *BMC Bioinformatics* 2008, **9**:559.

57. Betancur C: **Etiological heterogeneity in autism spectrum disorders: more than 100 genetic and genomic disorders and still counting**. *Brain Res* 2011, **1380**:42-77.

58. De Rubeis S, He X, Goldberg AP, Poultney CS, Samocha K, Cicek AE, Kou Y, Liu L, Fromer M, Walker S *et al*: **Synaptic, transcriptional and chromatin genes disrupted in autism**. *Nature* 2014, **515**(7526):209-215.

59. Gilman SR, Iossifov I, Levy D, Ronemus M, Wigler M, Vitkup D: **Rare de novo variants associated with autism implicate a large functional network of genes involved in formation and function of synapses**. *Neuron* 2011, **70**(5):898-907.

60. Iossifov I, O'Roak BJ, Sanders SJ, Ronemus M, Krumm N, Levy D, Stessman HA, Witherspoon KT, Vives L, Patterson KE *et al*: **The contribution of de novo coding mutations to autism spectrum disorder**. *Nature* 2014, **515**(7526):216-221.

61. Parikshak NN, Luo R, Zhang A, Won H, Lowe JK, Chandran V, Horvath S, Geschwind DH: **Integrative functional genomic analyses implicate specific molecular pathways and circuits in autism**. *Cell* 2013, **155**(5):1008-1021.

62. Pinto D, Delaby E, Merico D, Barbosa M, Merikangas A, Klei L, Thiruvahindrapuram B, Xu X, Ziman R, Wang Z *et al*: **Convergence of genes and cellular pathways dysregulated in autism spectrum disorders**. *Am J Hum Genet* 2014, **94**(5):677-694.

63. Wright CF, Fitzgerald TW, Jones WD, Clayton S, McRae JF, van Kogelenberg M, King DA, Ambridge K, Barrett DM, Bayzetinova T *et al*: **Genetic diagnosis of developmental disorders in**

the DDD study: a scalable analysis of genome-wide research data. *Lancet* 2015, **385**(9975):1305-1314.

64. Darnell JC, Van Driesche SJ, Zhang C, Hung KY, Mele A, Fraser CE, Stone EF, Chen C, Fak JJ, Chi SW *et al*: **FMRP stalls ribosomal translocation on mRNAs linked to synaptic function and autism**. *Cell* 2011, **146**(2):247-261.

65. Huang G, Chen S, Chen X, Zheng J, Xu Z, Doostparast Torshizi A, Gong S, Chen Q, Ma X, Yu J *et al*: **Uncovering the Functional Link Between SHANK3 Deletions and Deficiency in Neurodevelopment Using iPSC-Derived Human Neurons**. *Front Neuroanat* 2019, **13**:23.

66. Wang P, Lin M, Pedrosa E, Hrabovsky A, Zhang Z, Guo W, Lachman HM, Zheng D: **CRISPR/Cas9-mediated heterozygous knockout of the autism gene CHD8 and characterization of its transcriptional networks in neurodevelopment**. *Mol Autism* 2015, **6**:55.

67. Chen ES, Gigek CO, Rosenfeld JA, Diallo AB, Maussion G, Chen GG, Vaillancourt K, Lopez JP, Crapper L, Poujol R *et al*: **Molecular convergence of neurodevelopmental disorders**. *Am J Hum Genet* 2014, **95**(5):490-508.

68. Gigek CO, Chen ES, Ota VK, Maussion G, Peng H, Vaillancourt K, Diallo AB, Lopez JP, Crapper L, Vasuta C *et al*: **A molecular model for neurodevelopmental disorders**. *Transl Psychiatry* 2015, **5**:e565.

69. Zeng L, Zhang P, Shi L, Yamamoto V, Lu W, Wang K: **Functional impacts of NRXN1 knockdown on neurodevelopment in stem cell models**. *PLoS One* 2013, **8**(3):e59685.

70. Deneault E, White SH, Rodrigues DC, Ross PJ, Faheem M, Zaslavsky K, Wang Z, Alexandrova R, Pellecchia G, Wei W *et al*: **Complete Disruption of Autism-Susceptibility Genes by Gene Editing Predominantly Reduces Functional Connectivity of Isogenic Human Neurons**. *Stem Cell Reports* 2019, **12**(2):427-429.

71. Ha HTT, Leal-Ortiz S, Lalwani K, Kiyonaka S, Hamachi I, Mysore SP, Montgomery JM, Garner CC, Huguenard JR, Kim SA: **Shank and Zinc Mediate an AMPA Receptor Subunit Switch in Developing Neurons**. *Front Mol Neurosci* 2018, **11**:405.

72. Wu S, Gan G, Zhang Z, Sun J, Wang Q, Gao Z, Li M, Jin S, Huang J, Thomas U *et al*: **A Presynaptic Function of Shank Protein in Drosophila**. *J Neurosci* 2017, **37**(48):11592-11604.

73. Kozol RA, Cukier HN, Zou B, Mayo V, De Rubeis S, Cai G, Griswold AJ, Whitehead PL, Haines JL, Gilbert JR *et al*: **Two knockdown models of the autism genes SYNGAP1 and SHANK3 in zebrafish produce similar behavioral phenotypes associated with embryonic disruptions of brain morphogenesis**. *Hum Mol Genet* 2015, **24**(14):4006-4023.

74. Arons MH, Thynne CJ, Grabrucker AM, Li D, Schoen M, Cheyne JE, Boeckers TM, Montgomery JM, Garner CC: **Autism-associated mutations in ProSAP2/Shank3 impair synaptic transmission and neurexin-neuroligin-mediated transsynaptic signaling**. *J Neurosci* 2012, **32**(43):14966-14978.

75. Betancur C, Sakurai T, Buxbaum JD: **The emerging role of synaptic cell-adhesion pathways in the pathogenesis of autism spectrum disorders**. *Trends Neurosci* 2009, **32**(7):402-412.

76. Sudhof TC: **Neuroligins and neurexins link synaptic function to cognitive disease**. *Nature* 2008, **455**(7215):903-911.

77. Meyer G, Varoqueaux F, Neeb A, Oschlies M, Brose N: **The complexity of PDZ domain-mediated interactions at glutamatergic synapses: a case study on neuroligin**. *Neuropharmacology* 2004, **47**(5):724-733.

78. Budreck EC, Kwon OB, Jung JH, Baudouin S, Thommen A, Kim HS, Fukazawa Y, Harada H, Tabuchi K, Shigemoto R *et al*: **Neuroligin-1 controls synaptic abundance of NMDA-type glutamate receptors through extracellular coupling**. *Proc Natl Acad Sci U S A* 2013, **110**(2):725-730.

79. Harris KP, Akbergenova Y, Cho RW, Baas-Thomas MS, Littleton JT: **Shank Modulates Postsynaptic Wnt Signaling to Regulate Synaptic Development**. *J Neurosci* 2016, **36**(21):5820-5832.

80. Quesnel-Vallieres M, Weatheritt RJ, Cordes SP, Blencowe BJ: **Autism spectrum disorder: insights into convergent mechanisms from transcriptomics**. *Nat Rev Genet* 2019, **20**(1):51-63.

81. Kalkman HO: **A review of the evidence for the canonical Wnt pathway in autism spectrum disorders**. *Mol Autism* 2012, **3**(1):10.

82. Platt RJ, Zhou Y, Slaymaker IM, Shetty AS, Weisbach NR, Kim JA, Sharma J, Desai M, Sood S, Kempton HR *et al*: **Chd8 Mutation Leads to Autistic-like Behaviors and Impaired Striatal Circuits**. *Cell Rep* 2017, **19**(2):335-350.

83. Chenn A, Walsh CA: **Regulation of cerebral cortical size by control of cell cycle exit in neural precursors**. *Science* 2002, **297**(5580):365-369.

84. Dong F, Jiang J, McSweeney C, Zou D, Liu L, Mao Y: **Deletion of CTNNB1 in inhibitory circuitry contributes to autism-associated behavioral defects**. *Hum Mol Genet* 2016, **25**(13):2738-2751.

85. Krumm N, O'Roak BJ, Shendure J, Eichler EE: **A de novo convergence of autism genetics and molecular neuroscience**. *Trends Neurosci* 2014, **37**(2):95-105.

86. Frazier TW, Embacher R, Tilot AK, Koenig K, Mester J, Eng C: **Molecular and phenotypic abnormalities in individuals with germline heterozygous PTEN mutations and autism**. *Mol Psychiatry* 2015, **20**(9):1132-1138.

87. Spinelli L, Black FM, Berg JN, Eickholt BJ, Leslie NR: **Functionally distinct groups of inherited PTEN mutations in autism and tumour syndromes**. *J Med Genet* 2015, **52**(2):128-134.

88. Chen Y, Huang WC, Sejourne J, Clipperton-Allen AE, Page DT: **Pten Mutations Alter Brain Growth Trajectory and Allocation of Cell Types through Elevated beta-Catenin Signaling**. *J Neurosci* 2015, **35**(28):10252-10267.

89. Kwan V, Unda BK, Singh KK: **Wnt signaling networks in autism spectrum disorder and intellectual disability**. *J Neurodev Disord* 2016, **8**:45.

90. Snijders Blok L, Madsen E, Juusola J, Gilissen C, Baralle D, Reijnders MR, Venselaar H, Helsmoortel C, Cho MT, Hoischen A *et al*: **Mutations in DDX3X Are a Common Cause of Unexplained Intellectual Disability with Gender-Specific Effects on Wnt Signaling**. *Am J Hum Genet* 2015, **97**(2):343-352.

945 91. Gao C, Chen YG: **Dishevelled: The hub of Wnt signaling**. *Cell Signal* 2010, **22**(5):717-727.

946 92. Mines MA, Jope RS: **Brain region differences in regulation of Akt and GSK3 by chronic**
947 **stimulant administration in mice**. *Cell Signal* 2012, **24**(7):1398-1405.

948 93. Zhou WJ, Xu N, Kong L, Sun SC, Xu XF, Jia MZ, Wang Y, Chen ZY: **The antidepressant roles**
949 **of Wnt2 and Wnt3 in stress-induced depression-like behaviors**. *Transl Psychiatry* 2016,
950 **6**(9):e892.

951 94. Roh MS, Seo MS, Kim Y, Kim SH, Jeon WJ, Ahn YM, Kang UG, Juhnn YS, Kim YS: **Haloperidol**
952 **and clozapine differentially regulate signals upstream of glycogen synthase kinase 3 in the rat**
953 **frontal cortex**. *Exp Mol Med* 2007, **39**(3):353-360.

954 95. Launay JM, Mouillet-Richard S, Baudry A, Pietri M, Kellermann O: **Raphe-mediated signals**
955 **control the hippocampal response to SRI antidepressants via miR-16**. *Transl Psychiatry* 2011,
956 **1**:e56.

957 96. Sutton LP, Honardoust D, Mouyal J, Rajakumar N, Rushlow WJ: **Activation of the canonical Wnt**
958 **pathway by the antipsychotics haloperidol and clozapine involves dishevelled-3**. *J Neurochem*
959 2007, **102**(1):153-169.

960

961

DECLARATIONS

Acknowledgements. We would like to thank the families who kindly consented to participate in our study.

Funding. This work was supported by the Beatrice and Samuel A. Seaver Foundation. MSB is a Seaver Foundation Faculty Scholar and AB was a Seaver Graduate Fellow. In addition, MSB was funded by the Autism Science Foundation (#17-001) over the course of this work. JDB and ED were partially supported by NIMH grant MH111679. AB was also supported by a NICHD-Interdisciplinary Training Program in Systems and Developmental Biology and Birth Defects (T32 HD075735) and by a Neuroscience Training grant T32, jointly sponsored by NIMH and NINDS (T32 MH087004).

Authors' contributions. JDB, AB and ED conceived of the project. AB and ED prepared the iPSC lines, neuronal differentiation and RNA-seq samples. MSB performed the computational data analysis and wrote the manuscript with SS, GH, KB, JDB and ED. All authors edited and approved the final manuscript.

Ethics approval and consent to participate. All study participants have given written informed consent, and the genetic study has been approved by the Icahn School of Medicine at Mount Sinai Institutional Review Board.

Competing Interests. The authors declare no competing financial interests and no non-financial conflicts of interest for any of the authors.

MAIN TABLES

Table 1. Genetic and demographic information

Family ID	Proband Age (yrs)	Proband Sex	Sibling Age (yrs)	Sibling Sex	Race	Mutation type	Minimal deletion size	Chromosomal location
1	5	F	3	F	Caucasian	Frameshift	N/A	chr22:51160837-51160839 GCC/G
2	13	F	6	F	Caucasian	Deletion	42 kb	chr22:51,132,839-51,175,792
3	25	F	19	M	Caucasian/ American Indian	Deletion	43 kb	chr22:51,132,839-51,176,002
4	3	M	1	F	Caucasian	Deletion	62 kb	chr22:51,121,360-51,183,840
5	3	M	6	F	Caucasian	Deletion	85 kb	chr22:51,086,931-51,172,228
6	4	F	6	M	Asian	Deletion	4.98 Mb	chr22:46316673-51,304,566
7	9	F	12	M	Caucasian	Deletion	6.9 Mb	chr22:44321641-51,304,566*

Table 2. Overlap of PMS differentially expressed genes (FDR <5%) with exisiting ASD iPSC transcriptome studies.

Study description				iNPCs				iNeurons				Enriched GO terms (FDR <5%)
Author and year	Target gene	Approach	Cellular model	ET P-value	Odds ratio	Intersect	Example genes	ET P-value	Odds ratio	Intersect	Example genes	
Huang et., 2019	*SHANK3*	shRNA KD	hiPSC-derived neurons	**3.3E-04**	1.93	44	*COL5A2, COL18A1 NDP, ADAMTS18, CRTAP, NFATC1*	**2.4E-07**	4.64	20	*WNT3A, BCAN, FRZB, SPO3, APCDD1, WNT7B*	Wnt signaling, ECM, Signaling pathways regulating stem cell pluripotency
Wang et., 2015	*CHD8*	SPR/Cas9 heterozygous KO	hiPSC-derived NPCs	**4.0E-03**	1.71	33	*CCCND1, VCAN, NFATC1, SMAD9, LRRC8B, HOXB5*	**1.8E-05**	4.14	15	*FRZB, FREM1, RSPO3, ROR2, MMP15, WNT3A*	ECM, Wnt signaling, frizzled binding, netrin receptor activity, axon
	CHD8	SPR/Cas9 heterozygous KO	hiPSC-derived neurons	**1.3E-07**	1.95	91	*NKD2, COL5A2, COL18A1, NCAN, COL14A1, INHBE*	**5.7E-07**	3.48	29	*BCAN, FRZB, FREM1, RSPO3, ID1-3, WNT7B*	Non-canonical Wnt signaling pathway, ECM, Glypican pathway
Chen et., 2014	*TCF4*	shRNA KD	hiPSC-derived NPCs	6.2E-01	0.93	5	*ABCB4, FBXL15, SHF, NELL2, ADAMTSL1*	6.8E-01	0.89	1	*PLEKHA5*	NA
	EHMT1	shRNA KD	hiPSC-derived NPCs	**1.8E-03**	2.05	23	*NKD2, CAMK2A, COL18A1, VCAN, NCAN, HOXB6*	**1.8E-04**	4.52	10	*BCAN, ID2, ID1, WNT7B, ST6GALNAC3, CORO2B*	Perineuronal net, genes encoding proteoglycans and ECM, Hippo signaling pathway, Wnt signaling
Gigek et al., 2015	*MBD5*	shRNA KD	Human neural stem cells	8.8E-01	0.67	6	*NCAN, SMAD9, E2F7, MARCKSL1, IFITM3, TOP1MT*	5.6E-01	1.07	2	*ID1, KCNJ10*	Perineuronal net, ALK1 signaling
	SATB2	shRNA KD	Human neural stem cells	1.7E-01	1.41	11	*NCAN, HMGA2, KCND3, SIGMAR1, DDB2, GAD1*	**2.6E-04**	5.30	8	*BCAN, ID1, KCNIP1, KLF10, CORO2B, MPC1*	ECM proteoglycans, GABA synthesis, p53 signaling, Ras
Zeng et a.l., 2013	*NRXN1*	shRNA KD	Human neural stem cells	**1.3E-03**	4.06	8	*ZFHX3, NCAN, GFRA1, LRRC8B, DDB2, TMEM151B*	**4.2E-02**	4.68	4	*HSPA2, NKD2, COL5A2, KCNIP1*	Cell adhesion, neurogenesis, axonogenesis, cell motility, ECM
Deneault et al., 2018	*ATRX*	SPR/Cas9 heterozygous KO	iPSCs	**4.0E-02**	1.43	32	*SHANK3, CAMK2N1, INHBE, IGFBP3, SOCS2, GNB4*	**2.4E-02**	2.20	10	*BCAN, ID2, SHANK3, CAMK2N1, ST6GALNAC3, RHOU*	NA
	CHD8	SPR/Cas9 heterozygous KO		1.0E+00	0.00	0	-	2.4E-01	3.72	1	*OLIG3*	NA
	AFF2	SPR/Cas9 heterozygous KO		8.8E-01	0.55	2	*CRHBP, GRHL3*	5.4E-01	1.31	1	*HSPA2*	NA
	CACNA1C	ISPR/Cas9 homozygous KO		1.5E-01	1.72	6	*INHBE, GRID2, GPC6, SLC7A2, ADM2, CHMP6*	1.7E-01	2.71	2	*KLF10, ID2*	NA
	KCNQ2	ISPR/Cas9 homozygous KO		6.3E-01	1.01	1	*MDGA2*	1.0E+00	0.00	0	-	NA
	SCN2A	ISPR/Cas9 homozygous KO		**2.0E-04**	2.06	55	*CCND1, NKD2, COL5A2, VCAN, CRTAP, CAMK2A*	**1.7E-03**	2.56	16	*FRZB, ID1-3, HSPA2, SMOX, ST6GALNAC3,*	Voltage gated sodium channel activity, neuronal precursor
	ASTN2	ISPR/Cas9 homozygous KO		3.3E-01	1.33	5	*INHBE, FOXI3, STK32B, SEMA6D, MANEAL*	5.5E-01	1.25	1	*FOXB1*	Glycoproteins, ECM, Axon guidance
	DLGAP2	ISPR/Cas9 homozygous KO		9.3E-01	0.38	1	*IGFBP3*	1.0E-01	3.76	2	*ST6GALNAC3, RHOU*	NA
	TENM1	SPR/Cas9 heterozygous KO		1.8E-01	1.40	11	*CAMK2N1, SULT1C4, IGFBP3, CELSR1, MOCOS, FBXO25*	8.2E-01	0.59	1	*CAMK2N1*	NA
	ANOS1	SPR/Cas9 heterozygous KO		4.0E-01	1.46	2	*MDGA2, SHISA3*	1.0E+00	0.00	0	-	NA
	ATRX	SPR/Cas9 heterozygous KO	iPSC-derived neurons	**6.7E-07**	2.36	47	*CAMK2A, COL14A1, NCAN, GPC3, SHANK3, TSHZ2*	**2.1E-03**	2.88	12	*WNT3A, FRZB, GPC3, SHANK3, TSHZ2, ARHGAP20*	Glutamate receptor binding, Wnt signaling, synaptic signaling, glutamatergic synapse, postsynaptic
	CHD8	SPR/Cas9 heterozygous KO		1.0E+00	0.00	0		**2.7E-02**	8.27	2	*PCDHGA3, PCDHGA7*	NA
	AFF2	SPR/Cas9 heterozygous KO		3.9E-01	1.49	2	*IGFBP3, COL14A1*	**3.4E-02**	7.27	2	*SLITRK2, PIEZO2*	NA
	CACNA1C	ISPR/Cas9 homozygous KO		6.6E-01	0.94	1	*RASGRP1*	1.0E+00	0.00	0	-	NA
	KCNQ2	ISPR/Cas9 homozygous KO		1.0E+00	0.00	0	-	**1.3E-04**	17.19	4	*WNT3A, MSX2, PIEZO2, PCDHGA3*	NA
	SCN2A	ISPR/Cas9 homozygous KO		1.0E+00	0.00	0	-	**4.2E-02**	6.42	2	*PCDHGA3, PCDHGA7*	NA
	ASTN2	ISPR/Cas9 homozygous KO		1.0E+00	0.00	0	-	**3.3E-05**	15.20	5	*WNT3A, ID1, MSX2, PIEZO2, PCDHGA3*	NA
	DLGAP2	ISPR/Cas9 homozygous KO		1.0E+00	0.00	0	-	1.0E+00	0.00	0	-	NA
	TENM1	SPR/Cas9 heterozygous KO		2.9E-01	1.23	12	*GPC3, ARHGAP20, COL14A1, VCAN, SLC10A4, CAMSAP3*	**5.0E-03**	3.60	7	*WNT3A, ID1, MSX2, DPPA4, GPC3, ARHGAP20*	ECM, Glypican pathway, Wnt signaling, signaling patways regulating stem cell pluripotency
	ANOS1	SPR/Cas9 heterozygous KO		1.0E+00	0.00	0	-	**6.6E-03**	17.77	2	*WNT3A, PCDHGA3*	NA

A Fisher's exact test (FET) and an estimated odds-ratio were used to compute significance of each overlap. When the intersection is greater than six, an six intersecting example genes are displayed for brevity. Pathway level analyses were computed using overlapping genes and corrected for mulitple comparisons using the BH procedure in ToppGene. Abbreviations: KD, knockdown; KO, knockout.

MAIN FIGURES AND LEGENDS

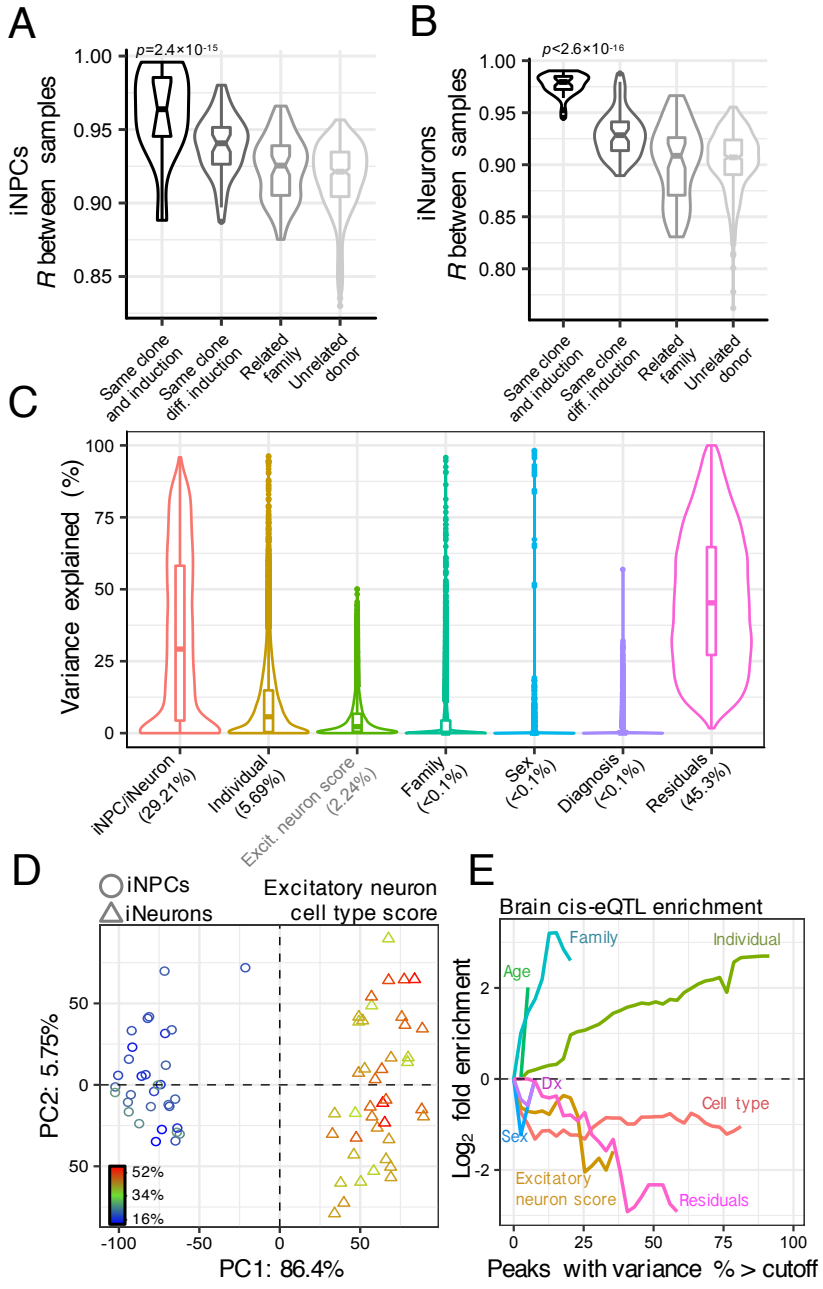

Figure 1. Quantifying transcriptome variance explained by observed factors. Correlation between samples from the same donor (technical replicates) compared to correlations between samples of related and unrelated family members in (**A**) iNPC and (**B**) iNeuron samples. Wilcoxon rank-sum test was used to test for differences between the means of correlation coefficients. (**C**) The linear mixed model

framework of the varianceParition R package was used to compute the percentage of gene expression variance explained according to seven covariates, which represent potential biological sources of variability. Differences in cell types and excitatory neuron cell composition (estimated using CiberSort in grey) explains the largest amount of variability in the transcriptome data. (**D**) Principal components analysis (PCA) of gene expression data from iNPCs (triangles) and iNeurons (circles) where samples are colored according to their predicted excitatory neuron cell type score. (**E**) Genes that vary most across donors are enriched for brain cis-eQTLs. Fold enrichment (log_2) for the 2000 top cis-eQTLs discovered in post mortem dorsolateral prefrontal cortex data generated by the CommonMind Consortium shown for seven sources of variation, plus residuals. Each line indicates the fold enrichment for genes with the fraction of variance explained exceeding the cutoff indicated on the *x*-axis. Enrichments are shown on the *x*-axis until less than 100 genes pass the cutoff.

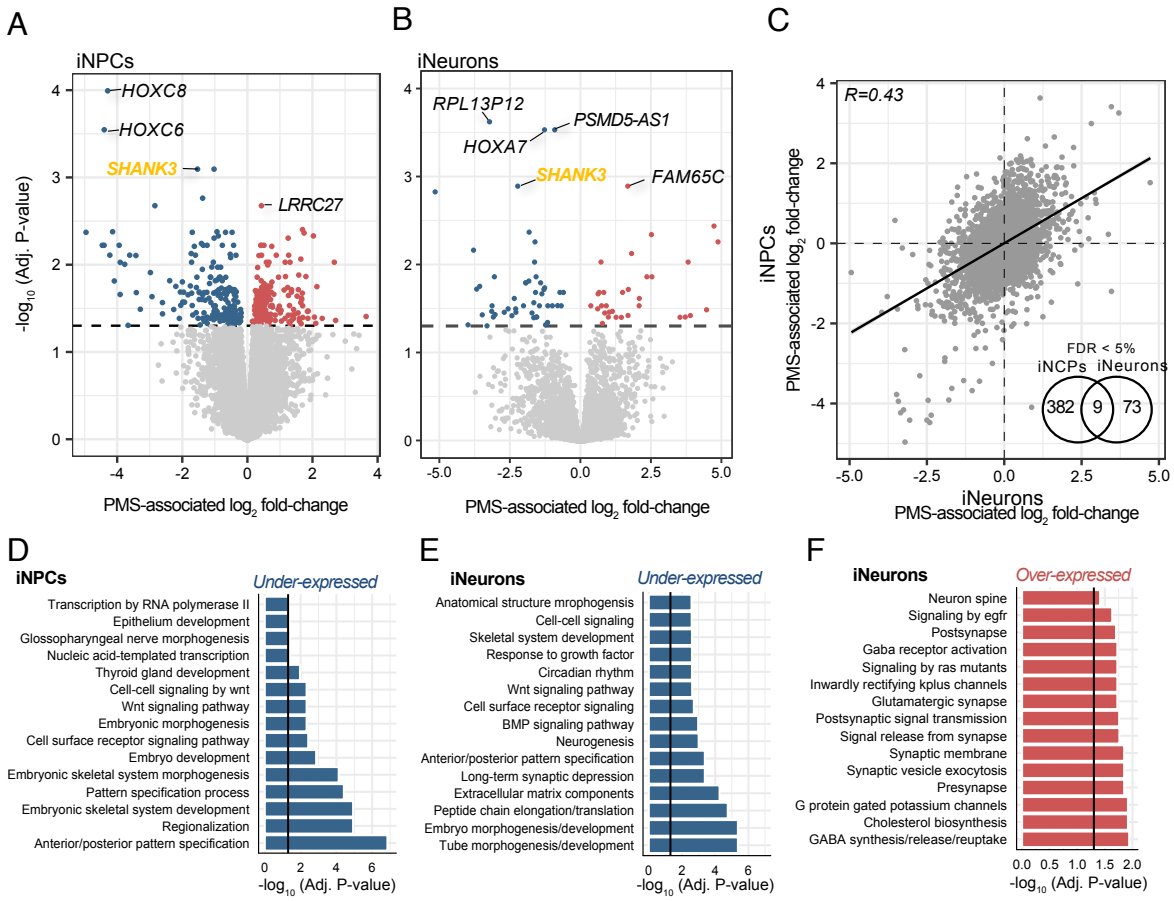

Figure 2. Genes and pathways associated with PMS. Differential gene expression analyses adjusted for sequencing batch, biological sex, RIN and individual donor as a repeated measure using the dupCorrelation function in the limma R package. Volcano plots compare the extent of PMS-associated log_2 fold-changes to $-log_{10}$ multiple test corrected *P*-value in (**A**) iNPCs and (**B**) iNeurons. Black dotted line indicates genes passing an adjusted P<0.05. (**C**) Genome-wide concordance of PMS-associated log_2 fold-changes was examined between iNCPs and iNeurons. Inset Venn diagram displays the overlap of significant differentially expressed genes between the two cell types. Functional enrichment analysis of PMS dysregulated genes that show (**D**) under-expression in iNPCs, (**E**) under-expression in iNeurons and (**F**) over-expression in iNeurons. All enrichment terms displayed pass a multiple test corrected *P*-value.

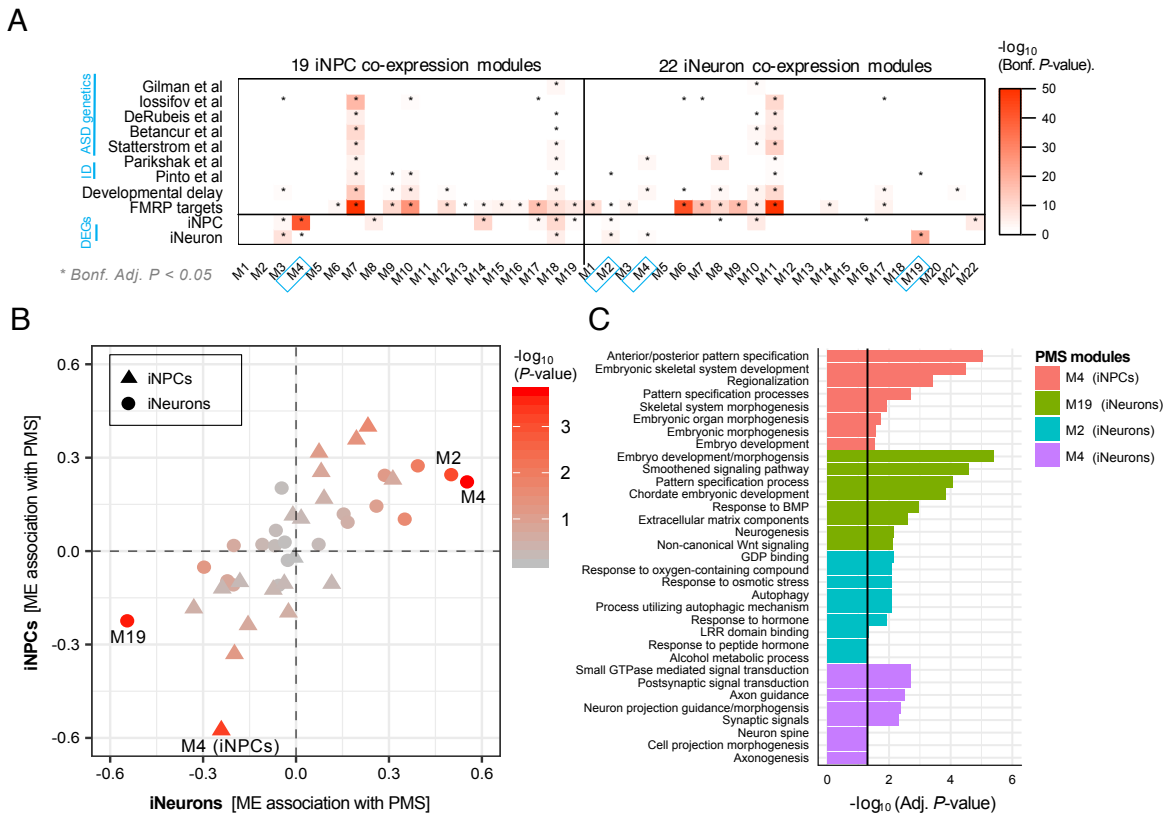

Figure 3. Genes co-expression analysis and enrichment. (**A**) A total of 19 co-expression modules were identified in iNPC samples and 22 modules were identified in iNeuron samples, and each module was tested for enrichment of genetic risk loci for ASD, ID and DD using findings from other large-scale studies. Modules were also examined for enrichment of target genes of FMRP, an RNA binding protein that is associated with ASD risk, as well as differentially expressed genes identified in the current study (see Figure 2). Enrichment was assessed using a Fisher's exact test to assess the statistical significance and *p*-values were adjusted for multiple testing using the Bonferroni procedure. We required an adjusted *P*-value < 0.05 (*) to claim that a gene set is enriched within a user-defined list of genes. (**B**) Module eigengene (ME) values were associated with PMS for iNPCs (triangles) and iNeurons (circles). Next, genes in the iNPC samples were then forced to construct modules using the gene-module assignments identified in the iNeuron samples, and vice versa, and these ME values were also associated with PMS.

(**C**) Functional enrichment was performed on four PMS-associated modules and the top eight enrichment terms (removing redundant annotations) are displayed.

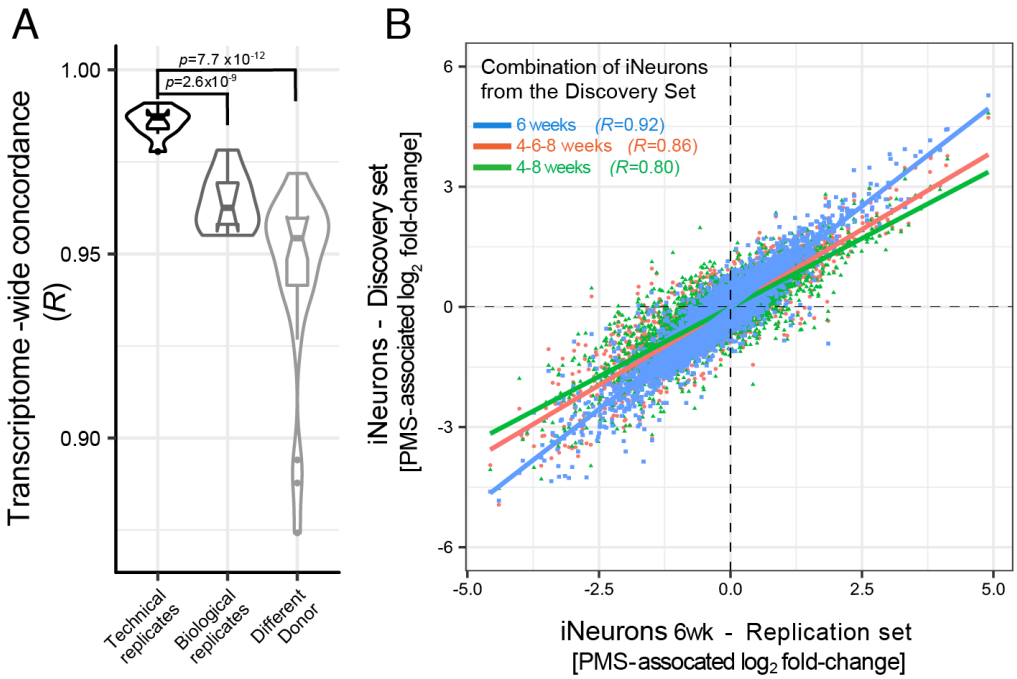

Figure 4. Replication of iNeuron RNA-seq. A replication set of iNeuron samples collected at 6 weeks in culture were subjected to RNA-seq. (**A**) Correlation coefficients between samples from the same donor and same clone (technical replicates), biological replicates from independent inductions and correlations between all other samples. A Wilcoxon rank-sum test was used to test for differences between the means of correlation coefficients. (**B**) The second replication batch of iNeuron samples were used to derive differential gene expression signatures between PMS probands and unaffected siblings. The PMS-associated $\log_2$ fold-changes from this replication set (x-axis) were compared to PMS-associated $\log_2$ fold-changes from the discovery set of samples, which were derived using combinations technical replicates and biological replicates at different weeks in culture (y-axis).

SUPPLEMENTAL FIGURES AND LEGENDS

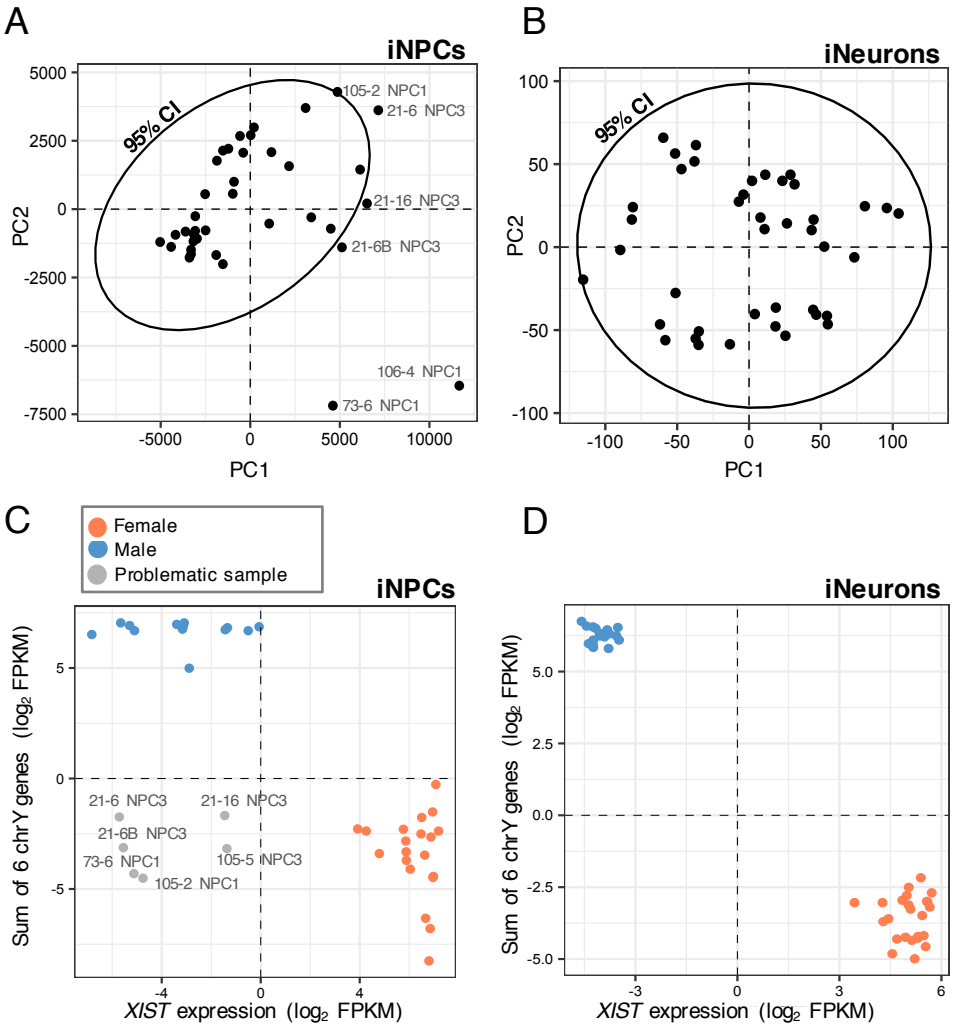

Figure S1. Outlier analyses. Principal component analyses were performed on RPKM values for all (**A**) iNPC and (**B**) iNeuron gene expression samples. Outliers beyond the 95% confidence intervals (black ellipse) were excluded from downstream analyses. We also sought to identify samples that may have under-gone issues with X-inactivation and/or sample mislabeling by confirming that the reported biological sex is concordant with gene expression on chrX and chrY for both (**C**) iNPC and (**D**) iNeuron samples. The expression on XIST from chrX was plotted against the sum of expression of six chrY genes

(*USP9Y*, *UTY*, *NLGN4Y*, *ZFY*, *RPS4Y1*, *TXLNG2P*). Female samples with intermediate expression profiles were excluded from further analysis.

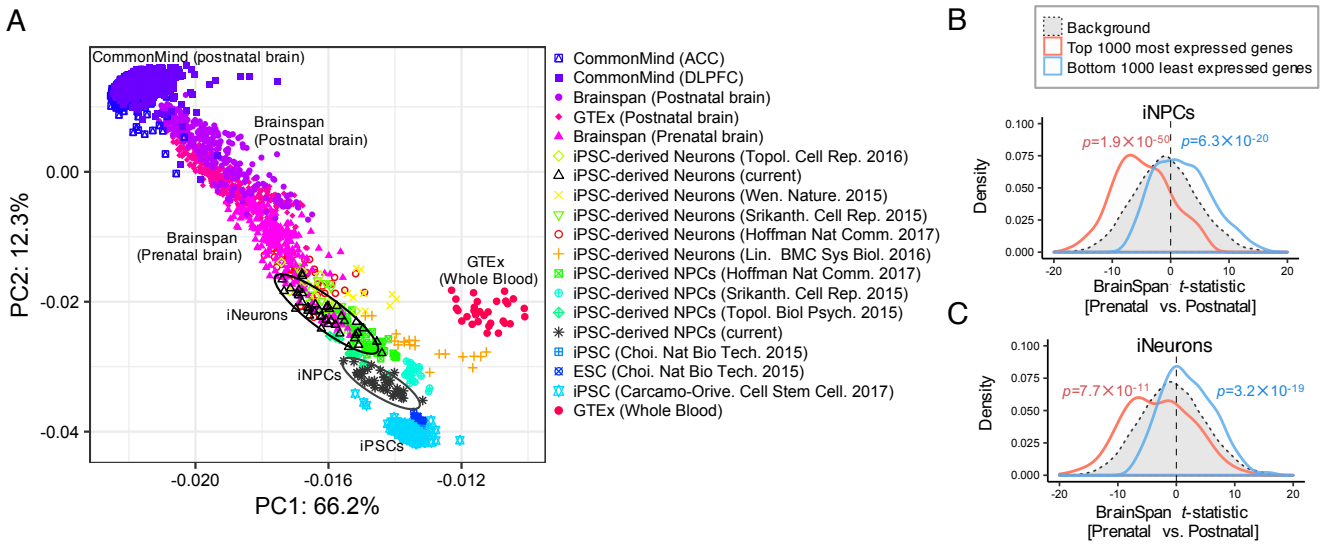

Figure S2. Developmental specificity analysis. (**A**) Several postmortem brain and hiPSC RNA-seq data sets spanning a broad range of developmentally distinct samples were integrated with the hiPSC-derived iNPCs and iNeurons in the current study by principal component analysis to confirm their developmental specificity. The first two principal components are shown and the iNPC samples (black stars) and iNeuron samples (black triangles) are each outlined by 95% confidence intervals. A t-statistic was calculated comparing prenatal to postnatal expression in the BrainSpan bulk RNA-seq data. (**B**) In iNPC samples, the t-statistic distribution of the top 1000 most expressed shows a prenatal bias and the top 1000 least expressed genes shows a clear postnatal bias. (**C**) A similar pattern was observed for the top 1000 most and least expressed genes across iNeuron samples.

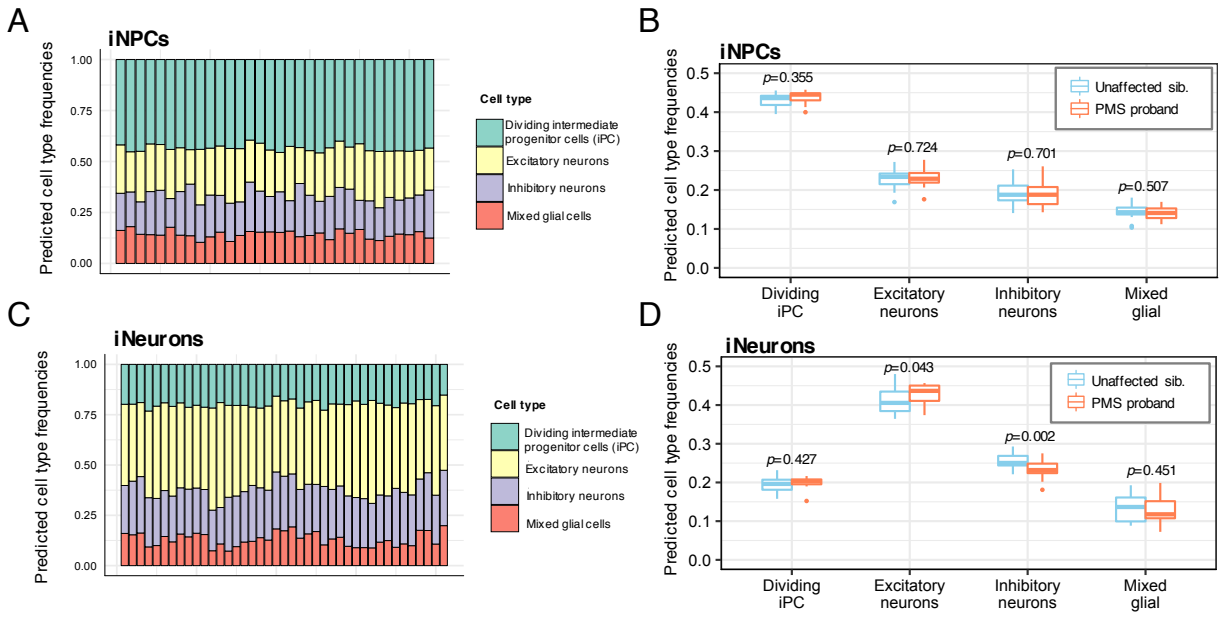

Figure S3. Cell type deconvolution analysis. Cibersort cell type deconvolution analysis of global gene expression profiles estimated cell frequencies (y-axis) in (**A-B**) iNPCs and (**C-D**) iNeurons for four major cell types (x-axis) using a reference panel of single-cell RNA-sequencing data from the human fetal cortex. The predicted cellular proportions were compared between PMS probands and unaffected siblings to confirm that major shifts in underlying cell types would not confound downstream analyses. A Wilcox rank-sum test was used to compare the fractions of cell proportions between probands and siblings.

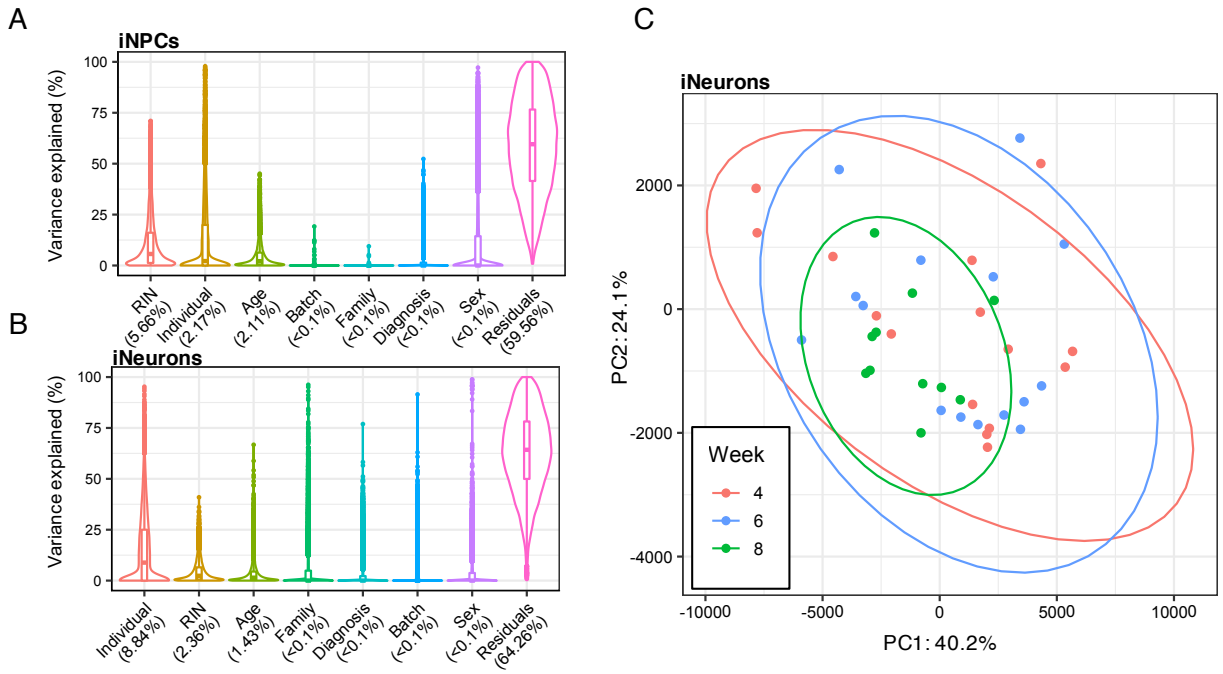

1082

1083 **Figure S4. Variance explained by technical factors.** The linear mixed model framework of the
1084 varianceParition R package was used to compute the percentage of gene expression variance explained by
1085 multiple biological and technical factors for (**A**) iNPCs and (**B**) iNeurons. (**C**) The variance explained by
1086 the total number of weeks iNeurons spent in culture was further evaluated by principal component
1087 analysis.

1088

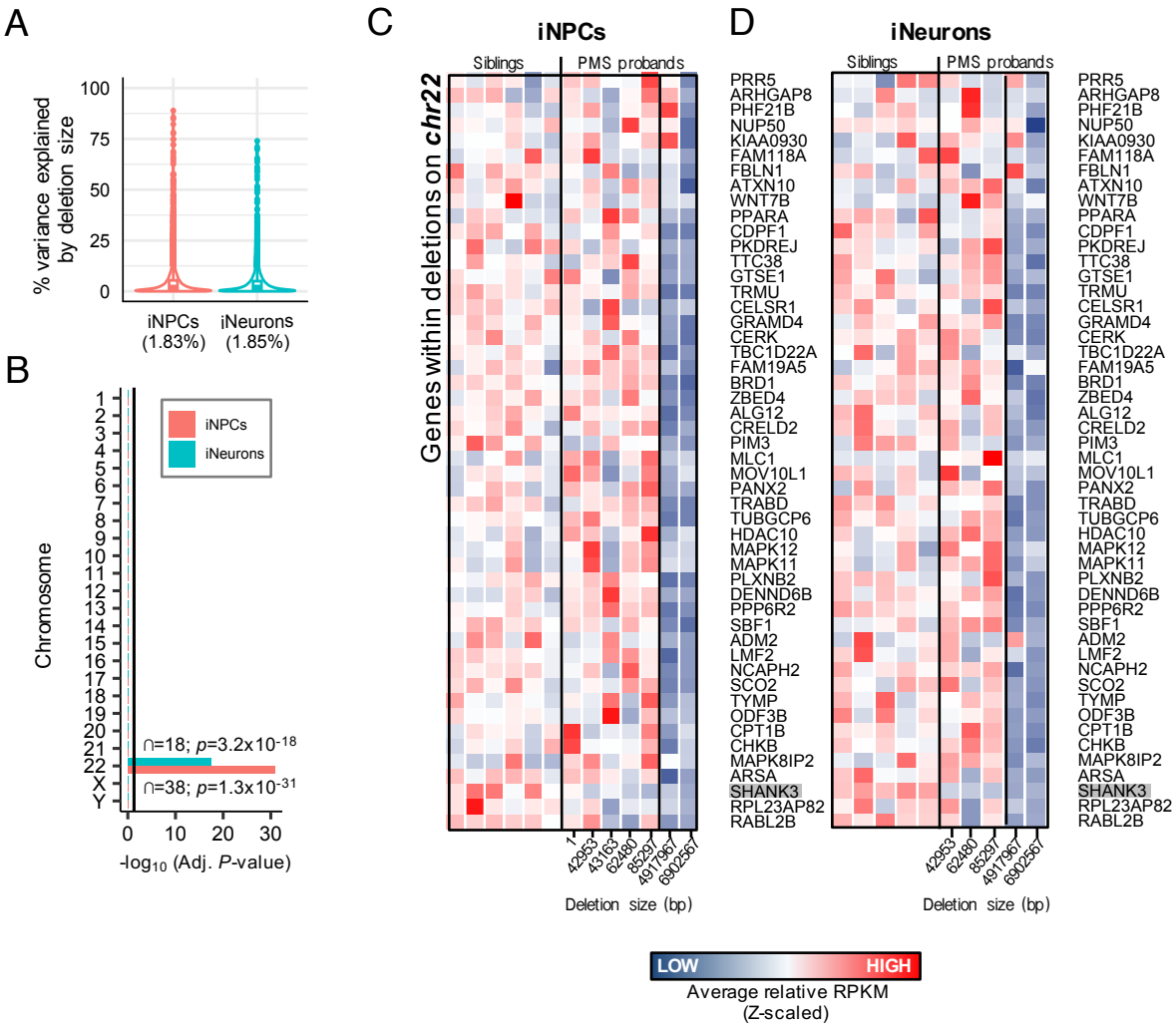

Figure S5. Variance explained by SHANK3 deletion size. (**A**) The linear mixed model framework of the varianceParition R package was used to compute the percentage of gene expression variance explained by SHANK3 deletion size in iNPCs and iNeurons. (**B**) Genes with variance explained >50% by deletion size were examined for chromosomal enrichment, and strong enrichment for chromosome 22 was observed. The vertical black line indicates -$\log_{10}$ P-value < 0.05. (**C**) Fifty unique genes were identified that varied by deletion size and mapped to chromosome 22, which were plotted on a heatmap using average expression values across all technical replicates for iNPC and iNeuron samples. The size of *SHANK3* deletion (bp) is displayed on the x-axis.

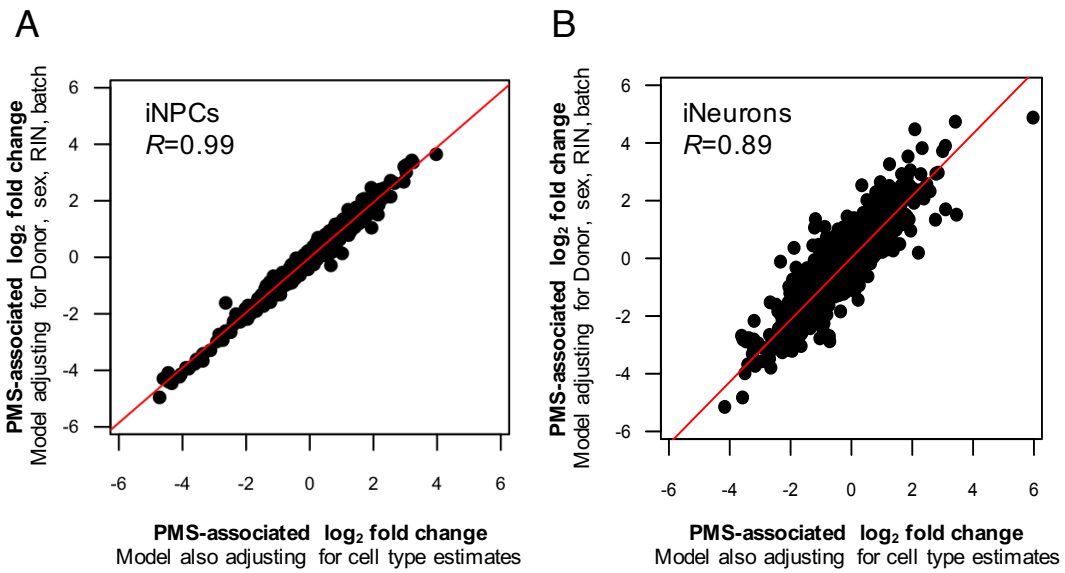

Figure S6. Controlling for cell type frequencies for differential expression. The concordance of genome-wide PMS-associated $\log_2$ fold-changes were evaluated comparing two models: i) one model adjusting for sequencing batch, biological sex, RIN and individual donor as a repeated measure on the y-axis; and ii) a second model adjusting for the same factors plus predicted excitatory neuron cell type composition on the x-axis. Concordance was examined for both (**A**) iNPC and (**B**) iNeuron samples.

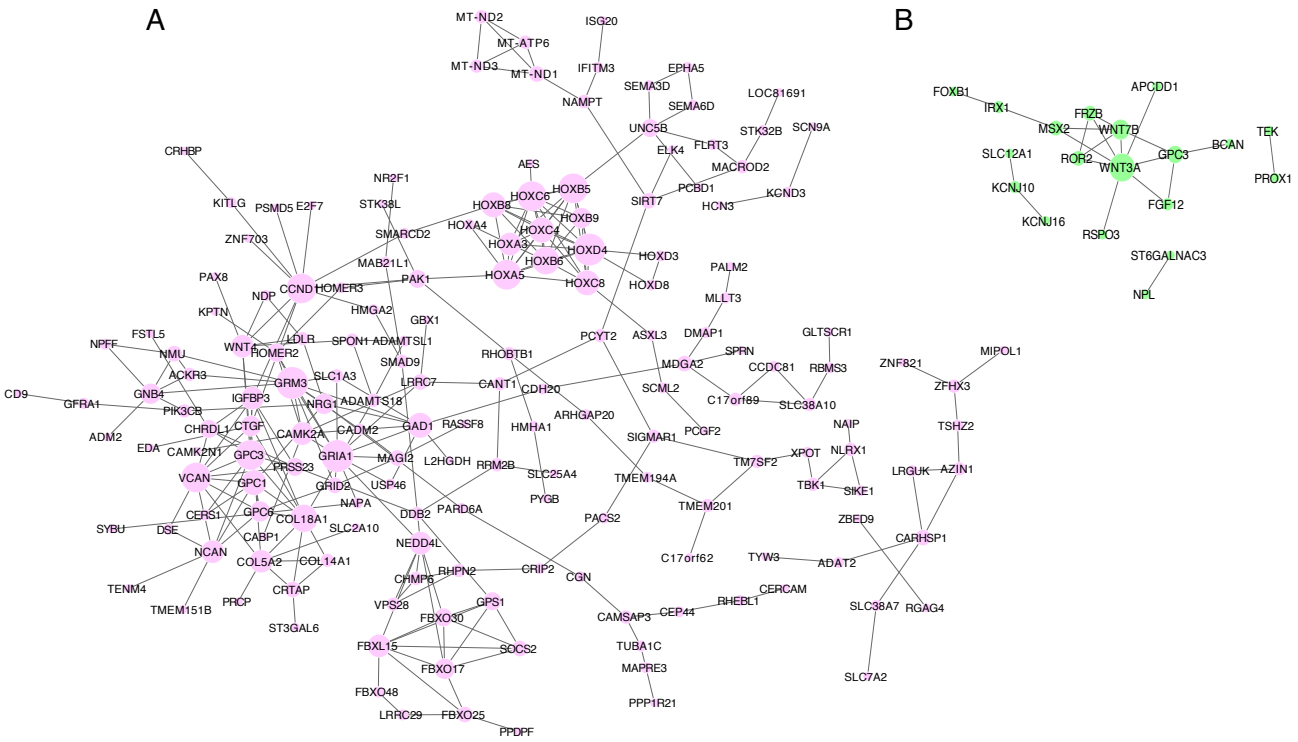

1107

1108 **Figure S7. Protein-protein interaction network.** Direct protein–protein interaction network of

1109 differentially expressed genes identified in (**A**) iNPCs and (**B**) iNeurons.

1110

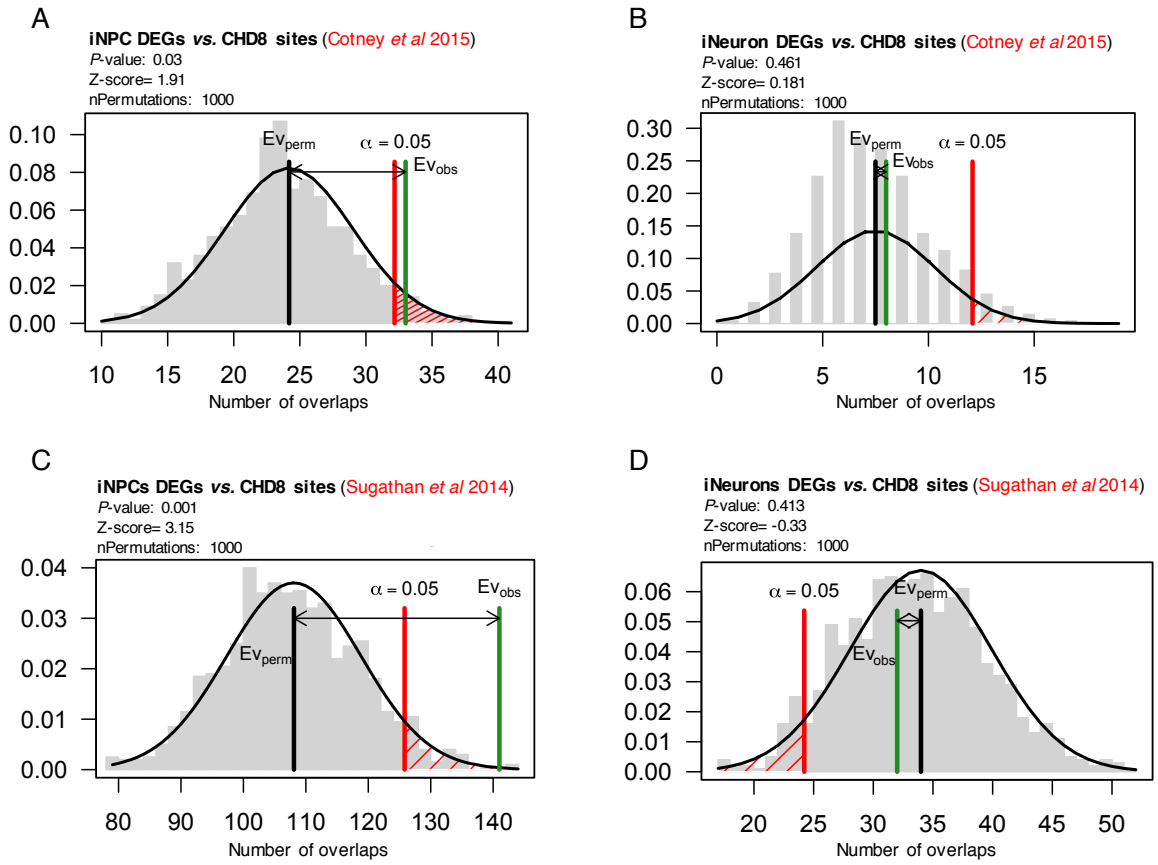

Figure S8. CHD8 enrichment analysis. Genomic coordinates for differentially expressed genes in iNPCs and iNeurons were assessed for enrichment for human brain specific CHD8 binding sites derived from (**A-B**) human mid-fetal brain tissue and (**C-D**) human neural progenitor cells (NPCs). The regioneR R package was used to test overlaps of genomic regions based on permutation sampling. We sampled random regions from the genome 1000 times, matching size and chromosomal distribution of the region set under study. By recomputing the overlap with *CHD8* binding sites in each permutation, statistical significance of the observed overlap was computed.

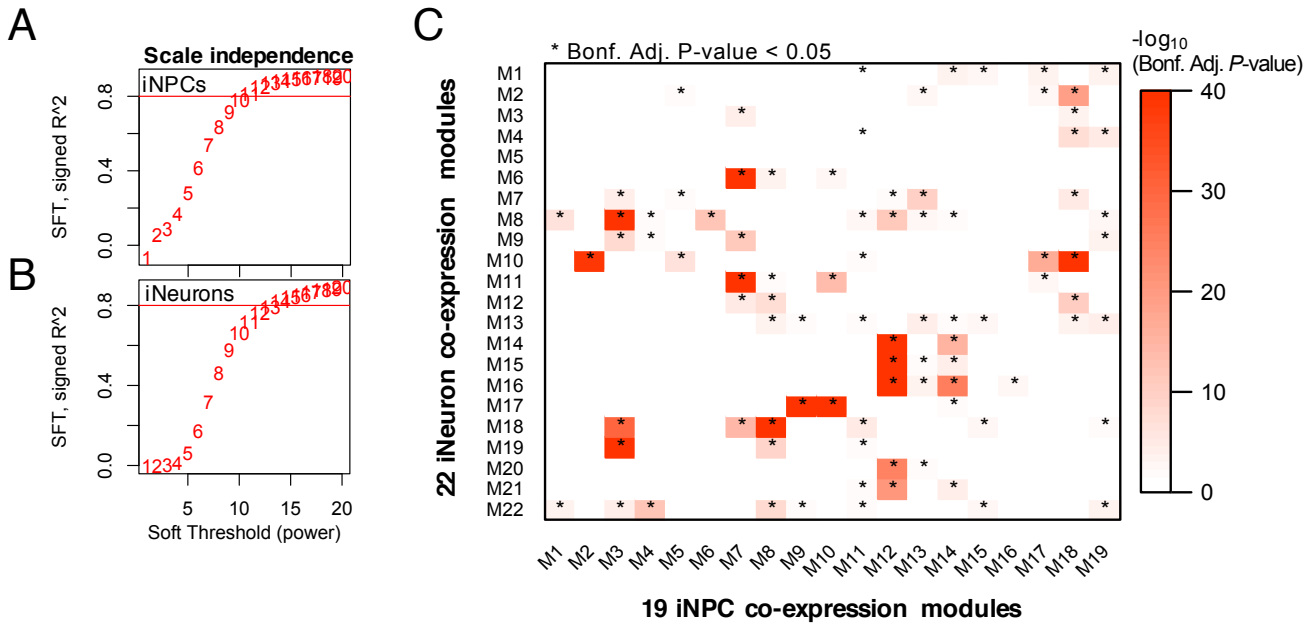

Figure S9. WGCNA module construction and overlap. The β-power defined for both (**A**) iNPC and (**B**) iNeuron samples in order to achieve scale free network topology for gene co-expression network construction. As a rule of thumb, β-power's > 0.8 achieve scale free network topology, and a final β-power of 12 was used iNPC samples and a β-power of 14 for iNeuron samples. (**C**) Overlap analysis of co-expression modules defined based on iNPC and iNeuron samples. Significance of the overlap was tested using a one-sided Fisher's exact test and corrected for multiple comparisons using Bonferroni procedure. Significant overlaps with adjusted P<0.05 are marked with an asterisks (*).

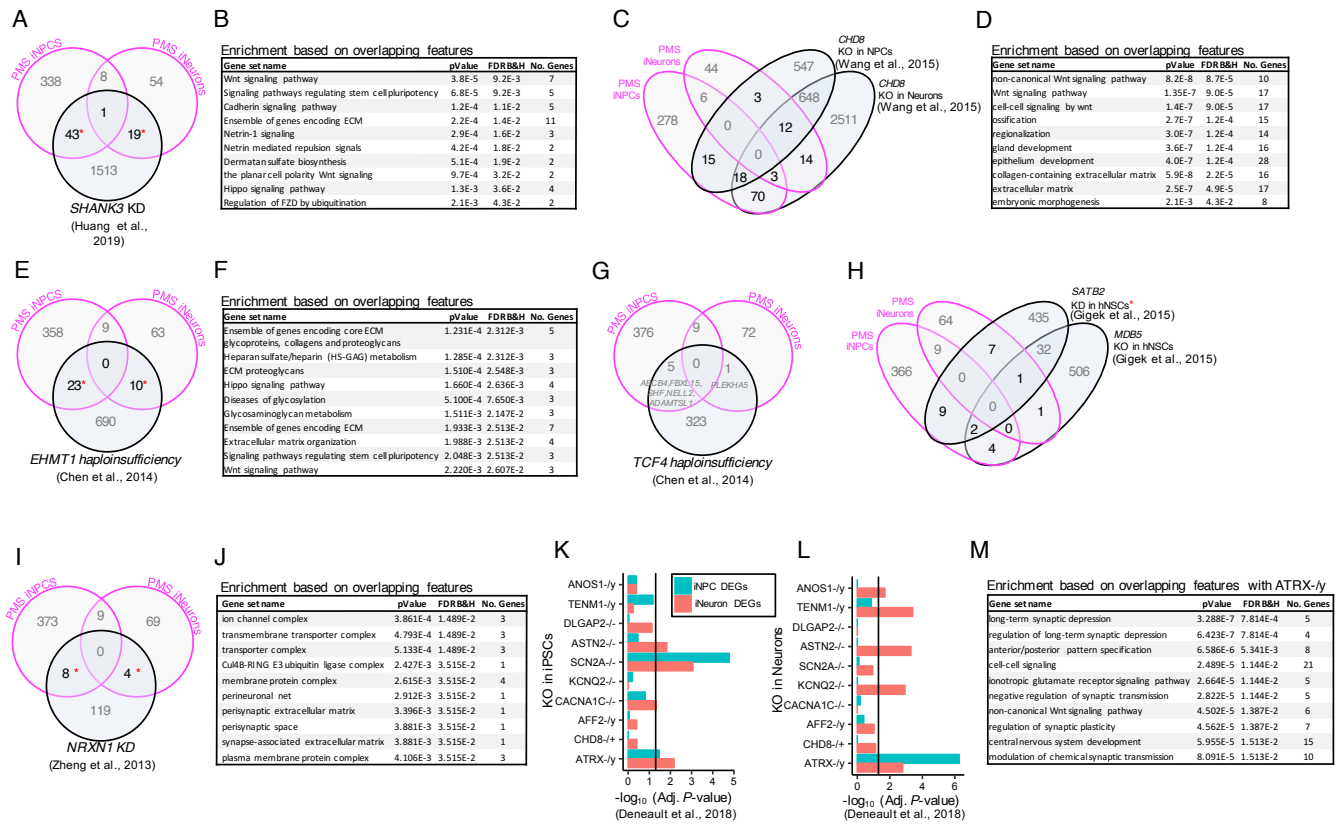

Figure S10. Overlap with other ASD iPSC transcriptome studies. Convergence of differentially expressed genes (FDR <5%) in the current study with other ASD iPSC transcriptome studies was assessed using a Fisher's Exact Test (FET) and an estimated odds-ratio was computed in comparison to a genome-wide background set to 20,000. Significant overlaps are demarked with a red asterisks (*). All overlapping genes found in common with the currents study were subjected to ToppGene functional enrichment. Overlap of differentially expressed genes and functional annotation was performed using data from (**A-B**) Huang et al., 2019, (**C-D**) Wang et al., 2015, and (**E-G**) Chen et al., 2014, (**H**) Gigek et al., 2015, (**I-J**) Zheng et al., 2013, and (**K-M**) Deneault et al., 2018. Note that no functional enrichment was observed based on the overlap with (**G**) Chen et al., 2014 and (**H**) Gigek et al., 2015. To simply multiple overlaps, (**K-L**) the -$\log_{10}$ P-value (x-axis) is used to display the extent of significance based on gene expression perturbations associated with CRISPR/Cas9 knockout of 10 different ASD genes.

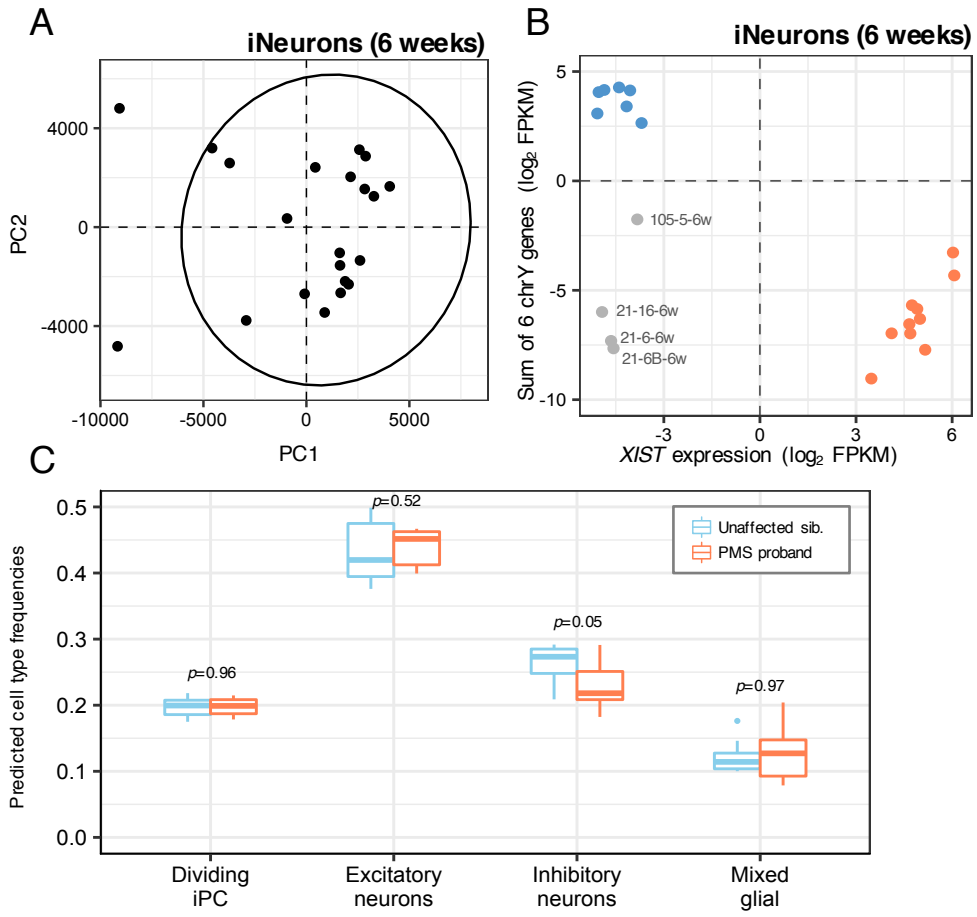

Figure S11. Data pre-processing using replication iNeuron samples. Principal component analyses were performed on RPKM values for (**A**) all replication set iNeuron samples at 6 weeks. Outliers beyond the 95% confidence intervals (black ellipse) were excluded from downstream analyses. (**B**) We also sought to identify samples that may have under-gone issues with X-inactivation and/or sample mislabeling by confirming that the reported biological sex is concordant with gene expression on chrX and chrY, which confirmed aberrant X-inactivation observed in iNPCs sharing the same clone and induction (*Supplemental Table 1*). Samples with intermediate expression profiles were excluded from further analysis. (**C**) Cibersort cell type deconvolution analysis of global gene expression profiles estimated cell frequencies (y-axis) for four major cell types (x-axis) using a reference panel of single-cell RNA-sequencing data from

1153 the human fetal cortex. The predicted cellular proportions were compared between PMS probands and
1154 unaffected siblings using a Wilcox rank-sum test.
1155
1156
1157
1158
1159
1160